

# Final-Model-Only Data Attribution with a Unifying View of Gradient-Based Methods

Dennis Wei\*   Inkit Padhi   Soumya Ghosh†  
Amit Dhurandhar   Karthikeyan Natesan Ramamurthy   Maria Chang

IBM Research

## Abstract

Training data attribution (TDA) is the task of attributing model behavior to elements in the training data. This paper draws attention to the common setting where one has access only to the final trained model, and not the training algorithm or intermediate information from training. To serve as a gold standard for TDA in this “final-model-only” setting, we propose *further training*, with appropriate adjustment and averaging, to measure the sensitivity of the given model to training instances. We then unify existing gradient-based methods for TDA by showing that they all approximate the further training gold standard in different ways. We investigate empirically the quality of these gradient-based approximations to further training, for tabular, image, and text datasets and models. We find that the approximation quality of first-order methods is sometimes high but decays with the amount of further training. In contrast, the approximations given by influence function methods are more stable but surprisingly lower in quality.

## 1 Introduction

Training data attribution (TDA, or sometimes simply “data attribution”) refers to the attribution or explanation of ML model behavior in terms of its training data. Existing methods for TDA can be broadly categorized into re-training-based approaches and gradient-based approaches. The former perform attribution by re-training on different subsets of training data and observing the corresponding effects (Ghorbani and Zou, 2019; Ghorbani et al., 2020; Feldman and Zhang, 2020; Kwon and Zou, 2022; Ilyas et al., 2022; Lin et al., 2022; Wang and Jia, 2023). The latter are in turn divided into those that track the effects of training instances throughout gradient-based training (Hara et al., 2019; Pruthi et al., 2020; Chen et al., 2021; Bae et al., 2024) versus those that are applied only at the end (Koh and Liang, 2017; Yeh et al., 2018; Koh et al., 2019; Barshan et al., 2020; Basu et al., 2020; Guo et al., 2021; Schioppa et al., 2022; Park et al., 2023; Kwon et al., 2024). We refer the reader to the survey by Hammoudeh and Lowd (2024) for a deeper look at these categories.

In this paper, rather than proposing another TDA method, we take a reflective approach to the literature. First, we draw attention to the fact that there exist multiple *problem settings* for TDA, alongside the multiple categories of methods. These problem settings differ in the level of access assumed. In particular, we focus on what we call the “final-model-only” (FiMO) setting in which we have access only to the final trained model, and not the algorithm used to train the model or

---

\*Correspondence to [dwei@us.ibm.com](mailto:dwei@us.ibm.com)

†Now with Merck Research Labs

intermediate information from training (for example checkpoints). The FiMO setting is motivated by the common scenario in which TDA is performed by a different party than the one who developed the model. This is the case for example for models downloaded from platforms such as HuggingFace.

We find that since the TDA literature has not clearly differentiated these problem settings, it is also not clear on what should be the ideal “gold standard” for TDA in the FiMO setting. Having a gold standard (as opposed to proxy tasks such as mislabelled example detection) facilitates the development and evaluation of more practical methods. We thus propose *further training*, starting from the given final model, as a gold standard measure of the sensitivity of the model to training instances. Our proposal adjusts for the effect of further training alone (as distinct from the effects of particular training instances) and accounts for the randomness of typical neural network training algorithms.

Like re-training<sup>1</sup>, further training a model multiple times can be computationally prohibitive. We thus consider approximations based on first- and second-order Taylor expansions of the further training objective. In doing so, we unify several existing gradient-based methods for TDA. These methods include gradient similarity (Charpiat et al., 2019) (a final-checkpoint-only case of TracIn (Pruthi et al., 2020)) and methods based on influence functions (Koh and Liang, 2017; Schioppa et al., 2022; Park et al., 2023; Grosse et al., 2023; Kwon et al., 2024). The direct connection that these gradient-based methods have to our further training objective suggests that they are more suited to the FiMO setting, rather than as approximations to re-training where their effectiveness has been questioned (Basu et al., 2021; Nguyen et al., 2023).

We investigate empirically the quality of the approximations to further training provided by different gradient-based methods. Our experiments span the modalities of tabular, image, and text data. Overall, we find that first-order gradient-based methods can give good initial approximations to further training, but the quality of approximation decays with the amount of further training. In contrast, the approximation quality of influence function methods is more persistent, but somewhat surprisingly, never as high as first-order methods at their peak.

Our contributions can be summarized as follows. 1) We highlight the FiMO setting for TDA (Section 2). 2) We articulate a further training gold standard for TDA in the FiMO setting (Section 3). 3) We show how several gradient-based TDA methods approximate further training, theoretically (Section 4) and numerically (Section 6). We discuss additional implications of our work in Section 7.

## 2 Problem Settings for Training Data Attribution

**Preliminaries** In all problem settings that we consider for training data attribution (TDA), we are given access to the training dataset  $\mathcal{D} = \{\mathbf{z}_i\}_{i=1}^n$  for the model, consisting of  $n$  pairs  $\mathbf{z}_i = (\mathbf{x}_i, y_i)$  of inputs  $\mathbf{x}_i \in \mathcal{X}$  and targets  $y_i \in \mathcal{Y}$ . A model  $f(\mathbf{x}; \boldsymbol{\theta})$  is a function  $f : \mathcal{X} \rightarrow \mathcal{F}$ , parameterized by  $\boldsymbol{\theta} \in \mathbb{R}^p$ , that maps to an output space  $\mathcal{F}$  (e.g., predicted logits for a classification model). The quality of each model output  $f(\mathbf{x}_i; \boldsymbol{\theta})$  with respect to target  $y_i$  is measured by a loss function  $\ell(f(\mathbf{x}_i; \boldsymbol{\theta}), y_i)$ ; we adopt the more compact notation  $L(\mathbf{z}_i; \boldsymbol{\theta}) \triangleq \ell(f(\mathbf{x}_i; \boldsymbol{\theta}), y_i)$ . We use  $A$  to denote the *training algorithm* or *learning algorithm* used to train  $f(\mathbf{x}; \boldsymbol{\theta})$  on dataset  $\mathcal{D}$ . We view  $A$  as a function that takes  $\mathcal{D}$  and initial model parameters  $\boldsymbol{\theta}^{(0)}$  (which may come from a pre-trained model) as input and outputs final model parameters  $\boldsymbol{\theta}^f = A(\mathcal{D}, \boldsymbol{\theta}^{(0)})$ . The algorithm  $A$  may be stochastic, for example due to the random ordering of instances in each training epoch.

Given a test instance  $\mathbf{z} = (\mathbf{x}, y)$  and an *evaluation function*  $g(\mathbf{z}, \boldsymbol{\theta})$  that depends in general on both  $f(\mathbf{x}; \boldsymbol{\theta})$  and  $y$ , the task of TDA is to assign scores  $a_i$  quantifying the importance of each training instance  $\mathbf{z}_i$  to the output  $g(\mathbf{z}, \boldsymbol{\theta})$ . We refer to  $a_i$  interchangeably as an attribution or influence score.

---

<sup>1</sup>Throughout the paper, we reserve the term “re-training” to mean re-training from scratch.

Commonly, the evaluation function is the loss on  $\mathbf{z}$ ,  $g(\mathbf{z}, \boldsymbol{\theta}) = L(\mathbf{z}; \boldsymbol{\theta})$ , or the output of the model alone,  $g(\mathbf{z}, \boldsymbol{\theta}) = f(\mathbf{x}; \boldsymbol{\theta})$ . One may also consider evaluation functions that sum over test instances, i.e.,  $\sum_{\mathbf{z} \in \mathcal{D}_{\text{test}}} g(\mathbf{z}, \boldsymbol{\theta})$ .

**Three problem settings** We distinguish three problem settings for TDA, based on the level of access to the above-defined quantities:

1. **Training Algorithm Available (TAA)**: In this first case, we have access to the training algorithm  $A$ . TDA can therefore be done by re-training the model on (i.e., applying  $A$  to) different subsets of  $\mathcal{D}$  and evaluating the resulting effects. This scenario typically occurs when the parties training the model and performing data attribution are the same.
2. **Checkpoints Available (CPA)**: We do not have access to  $A$  but do have intermediate information from the training process, for example intermediate model parameters  $\boldsymbol{\theta}^{(t)}$  (i.e., “checkpoints”) or gradients  $\nabla_{\boldsymbol{\theta}} f(\mathbf{x}_i; \boldsymbol{\theta}^{(t)})$ , as well as algorithm details such as learning rates. Here, TDA can be done by “tracing” the effect of training instances throughout the process. This scenario is also more typical when model training and data attribution are performed by the same party.
3. **Final Model Only (FiMO)**: We have access only to the final model  $f(\mathbf{x}; \boldsymbol{\theta}^f)$  and not the training algorithm  $A$  or intermediate information. The algorithm  $A$  may be actually unavailable, or it may be available but too computationally expensive or otherwise undesirable to re-run. This scenario typically occurs when model training and data attribution are performed by different parties.

The three settings also differ in the object whose behavior is being attributed. In the TAA setting, the object is the algorithm  $A$  and its sensitivity to different training instances  $\mathbf{z}_i$ . In the CPA setting, it is the training trajectory. The FiMO setting is the most focused on the final model  $f(\mathbf{x}; \boldsymbol{\theta}^f)$  that will actually be used.

In the remainder of the paper, we focus on the FiMO setting as it requires the least amount of access and is thus the most widely applicable. It applies for example to open-weights models that are freely downloadable from platforms such as HuggingFace. By extension, the FiMO setting applies in cases where methods for the TAA and CPA settings (i.e., re-training and tracing methods) cannot be used.

### 3 A Further Training Gold Standard for the FiMO Setting

We first consider the question of how TDA should ideally be done in the FiMO setting, i.e., what could serve as a “gold standard” method. While a gold standard method may be very expensive to carry out in many cases, it is nevertheless useful in evaluating and developing approximate TDA methods that are more practical. However, since the TDA literature has not explicitly delineated the FiMO setting to our knowledge, it is also not clear what the gold standard should be.

Returning for a moment to the TAA setting where the training algorithm is available, the natural question to ask there is one of *contribution*: how much does a training instance  $\mathbf{z}_i$  contribute to the model through the training process? Accordingly, variants of re-training, designed to estimate these contributions, are accepted as gold standards in the TAA setting. The simplest of these is leave-one-out (LOO) re-training where each instance  $\mathbf{z}_i$  is left out of the training set in turn to assess its contribution. In the FiMO setting however, it is not clear how one can “go back in time” to determine contributions to the final model. Instead, we change the question to one of *sensitivity*:

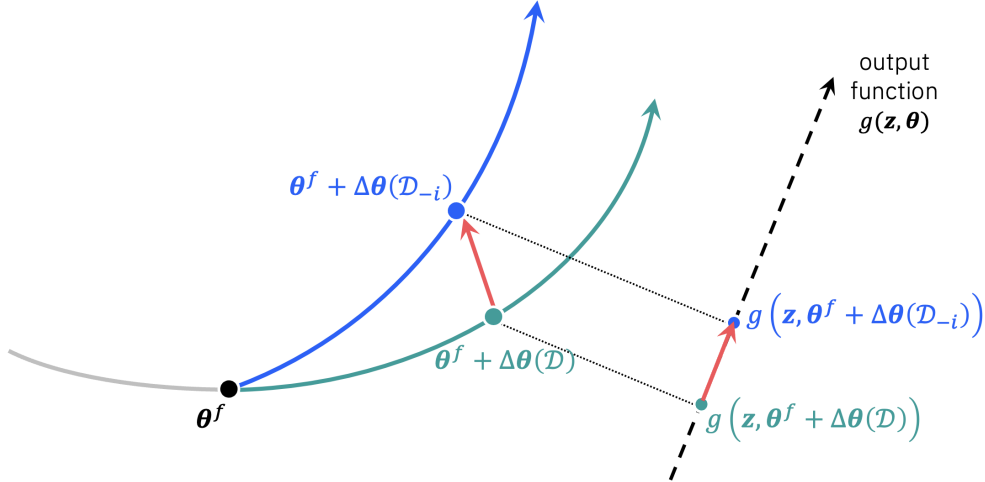


Figure 1: Given only a final model with parameters  $\theta^f$ , the proposed *further training* gold standard measures the model’s sensitivity to training sample  $i$  by conducting a limited amount of further training on the full training set  $\mathcal{D}$  as well as leaving out sample  $i$  ( $\mathcal{D}_{-i}$ ), resulting in changed parameters  $\theta^f + \Delta\theta(\mathcal{D})$  and  $\theta^f + \Delta\theta(\mathcal{D}_{-i})$ . The difference in outputs  $g(z, \theta^f + \Delta\theta(\mathcal{D}_{-i})) - g(z, \theta^f + \Delta\theta(\mathcal{D}))$  between the two further trained models indicates the sensitivity to  $i$ . If training is stochastic, then this process should be repeated to obtain the expected sensitivity.

how sensitive is the given model to a training instance  $z_i$ ? To measure these sensitivities, we propose variants of *further training* as a gold standard, in a manner analogous to how re-training is used in the TAA setting.

Further training can be described generically as follows. We start from the given parameters  $\theta^f$  and train on a dataset  $\mathcal{D}'$  using an algorithm  $A'$ , i.e.,  $\theta^f + \Delta\theta = A'(\mathcal{D}', \theta^f)$ , where  $\mathcal{D}'$  and  $A'$  are generally different from  $\mathcal{D}$  and  $A$ . In this work, we restrict attention to LOO further training, corresponding to LOO datasets  $\mathcal{D}' = \mathcal{D}_{-i} \triangleq \mathcal{D} \setminus \{z_i\}$  as well as  $\mathcal{D}' = \mathcal{D}$ , but more general perturbed datasets  $\mathcal{D}'$  are possible. As for  $A'$ , our desire is for it to be representative of typical neural network (NN) training. We thus assume that  $A'$  seeks to minimize the empirical risk  $R(\mathcal{D}'; \theta) \triangleq \sum_{z_i \in \mathcal{D}'} L(z_i; \theta)$ :

$$\Delta\theta(\mathcal{D}') \approx \arg \min_{\Delta\theta} R(\mathcal{D}'; \theta^f + \Delta\theta), \quad (1)$$

where the notation  $\theta^f + \Delta\theta$  is meant to indicate that the optimization is initialized at  $\theta^f$  ( $\Delta\theta = \mathbf{0}$ ), and  $\Delta\theta(\mathcal{D}')$  is the change in parameters resulting from applying  $A'$  to  $(\mathcal{D}', \theta^f)$ .

With further training as a building block, we now address two issues inherent to typical NN training.<sup>2</sup>

**Non-convergence:** The “final” parameters  $\theta^f$  are often not a stationary point of the empirical risk. Hence, as shown in Figure 1, further training on the original training set  $\mathcal{D}' = \mathcal{D}$  generally yields a non-zero change  $\Delta\theta(\mathcal{D})$ . This parameter shift is reflected in the evaluation function as  $g(z, \theta^f + \Delta\theta(\mathcal{D}))$  and can be interpreted as the effect due to further training alone. Similarly,  $\Delta\theta(\mathcal{D}_{-i})$  and  $g(z, \theta^f + \Delta\theta(\mathcal{D}_{-i}))$  in Figure 1 are the effects of further training without instance  $z_i$ .

<sup>2</sup>For convex training objectives, these issues are not much of a concern. Moreover, further training and re-training are essentially equivalent (please see Appendix A).

The difference in outputs,

$$g(\mathbf{z}, \boldsymbol{\theta}^f + \Delta\boldsymbol{\theta}(\mathcal{D}_{-i})) - g(\mathbf{z}, \boldsymbol{\theta}^f + \Delta\boldsymbol{\theta}(\mathcal{D})), \quad (2)$$

can therefore be interpreted as the sensitivity to the presence of  $\mathbf{z}_i$ , where we have adjusted for the effect of further training alone.

**Stochasticity of training:** The training algorithm  $A'$  also depends on random elements, notably the order of instances in each training epoch. Denoting these random elements as  $\xi$ , the change in parameters becomes a function of  $\xi$ ,  $\boldsymbol{\theta}^f + \Delta\boldsymbol{\theta}(\mathcal{D}', \xi) = A'(\mathcal{D}', \boldsymbol{\theta}^f, \xi)$ , as does the evaluation function  $g(\mathbf{z}, \boldsymbol{\theta}^f + \Delta\boldsymbol{\theta}(\mathcal{D}', \xi))$ . We view  $\xi$  as a nuisance parameter, an artifact of the stochastic nature of modern training algorithms. Thus, we would ideally like to take an expectation over  $\xi$ . Applying this to the difference in (2) yields

$$a_i^* = \mathbb{E} \left[ g(\mathbf{z}, \boldsymbol{\theta}^f + \Delta\boldsymbol{\theta}(\mathcal{D}_{-i}, \xi)) - g(\mathbf{z}, \boldsymbol{\theta}^f + \Delta\boldsymbol{\theta}(\mathcal{D}, \xi)) \right] \quad (3)$$

as the *adjusted* and *expected* sensitivity to leaving out instance  $\mathbf{z}_i$ . Equation (3) is our proposed gold standard attribution score based on further training.

## 4 Gradient-Based Methods as Approximate Further Training

The further training gold standard described in the previous section is computationally expensive. In the case of LOO further training, the number of further trainings scales with the training set size  $n$ , or at least the number of training instances for which we wish to estimate attribution scores. If we wish to approximate the expectation in (3) by averaging over multiple realizations of  $\xi$ , that further scales the cost. It is natural therefore to consider approximate further training. In this section, we assume that the amount of further training is limited, so that the resulting changes in model parameters,  $\Delta\boldsymbol{\theta}$ , are small. We show that several gradient-based methods for TDA can be re-derived from this perspective. This suggests that they are better viewed as approximations to further training and better suited to sensitivity analysis in the FiMO setting than for other purposes. It is important to note that we do not assume the given parameters  $\boldsymbol{\theta}^f$  are a stationary point for training set  $\mathcal{D}$ .

### 4.1 Approximate further training

The assumption that  $\Delta\boldsymbol{\theta}$  is small leads us to consider first- and second-order Taylor expansions of (1):

$$\widehat{\Delta\boldsymbol{\theta}}(\mathcal{D}') = \arg \min_{\Delta\boldsymbol{\theta}} R(\mathcal{D}'; \boldsymbol{\theta}^f) + \left( \nabla_{\boldsymbol{\theta}} R(\mathcal{D}'; \boldsymbol{\theta}^f) \right)^T \Delta\boldsymbol{\theta} + \frac{1}{2} \Delta\boldsymbol{\theta}^T \nabla_{\boldsymbol{\theta}}^2 R(\mathcal{D}'; \boldsymbol{\theta}^f) \Delta\boldsymbol{\theta} + \frac{\lambda}{2} \|\Delta\boldsymbol{\theta}\|_2^2, \quad (4)$$

where  $\nabla_{\boldsymbol{\theta}} R(\mathcal{D}'; \boldsymbol{\theta}^f)$  and  $\nabla_{\boldsymbol{\theta}}^2 R(\mathcal{D}'; \boldsymbol{\theta}^f)$  denote the gradient and Hessian of the empirical risk with respect to  $\boldsymbol{\theta}$  evaluated at  $\boldsymbol{\theta} = \boldsymbol{\theta}^f$ , and the first-order expansion omits the Hessian term. In both cases, an  $\ell_2$  regularizer  $(\lambda/2)\|\Delta\boldsymbol{\theta}\|_2^2$  has been added in (4), corresponding to the ‘‘damping’’ term in influence function estimation. As discussed in Appendix B.1, the regularizer can be motivated in two ways: 1) enforcing the smallness of  $\Delta\boldsymbol{\theta}$  and the accuracy of the Taylor expansion; 2) ensuring that solutions to (4) do not diverge. To achieve 2), we make the following assumption.

**Assumption 1.** If the Hessian  $\nabla_{\boldsymbol{\theta}}^2 R(\mathcal{D}'; \boldsymbol{\theta}^f)$  is present in (4), then  $\lambda > -\lambda_{\min}(\nabla_{\boldsymbol{\theta}}^2 R(\mathcal{D}'; \boldsymbol{\theta}^f))$ , where  $\lambda_{\min}$  denotes the minimum eigenvalue.

We may similarly expand the evaluation function  $g(\mathbf{z}, \boldsymbol{\theta}^f + \Delta\boldsymbol{\theta})$  to first order in  $\Delta\boldsymbol{\theta}$ . Doing so reduces the difference in (2) to the inner product

$$\hat{\alpha}_i = (\nabla_{\boldsymbol{\theta}} g(\mathbf{z}, \boldsymbol{\theta}^f))^T (\widehat{\Delta\boldsymbol{\theta}}(\mathcal{D}_{-i}) - \widehat{\Delta\boldsymbol{\theta}}(\mathcal{D})). \quad (5)$$

## 4.2 First-order methods

**First-order expansion recovers Grad-Dot** In the case of first-order Taylor expansion, the absence of the Hessian term in (4) makes its solution straightforward. For  $\mathcal{D}' = \mathcal{D}$ , we have  $\widehat{\Delta\boldsymbol{\theta}}(\mathcal{D}) = -\lambda^{-1} \nabla_{\boldsymbol{\theta}} R(\mathcal{D}, \boldsymbol{\theta}^f)$ , and similarly  $\widehat{\Delta\boldsymbol{\theta}}(\mathcal{D}_{-i}) = -\lambda^{-1} (\nabla_{\boldsymbol{\theta}} R(\mathcal{D}, \boldsymbol{\theta}^f) - \nabla_{\boldsymbol{\theta}} L(\mathbf{z}_i, \boldsymbol{\theta}^f))$ . Hence (5) becomes

$$\hat{\alpha}_i = \lambda^{-1} (\nabla_{\boldsymbol{\theta}} g(\mathbf{z}, \boldsymbol{\theta}^f))^T \nabla_{\boldsymbol{\theta}} L(\mathbf{z}_i, \boldsymbol{\theta}^f), \quad (6)$$

which is proportional to the inner product between training loss and test evaluation gradients. This corresponds to the ‘‘Grad-Dot’’ method (Charpiat et al., 2019), and also to a special case of TracIn (Pruthi et al., 2020) that uses only the final checkpoint. Here the damping value  $\lambda$  turns out not to matter because it is an overall constant of proportionality. A variation is to use the cosine similarity between gradients (‘‘Grad-Cos’’) instead of the unnormalized inner product.

## 4.3 Influence function methods

To show that the approximate further training formulation in (4), (5) recovers influence function-based TDA methods, we first present two ingredients: influence functions for (4), and the Gauss-Newton approximation to the Hessian that is commonly made.

### 4.3.1 Influence functions for (4)

Influence functions approximate the effect of down-weighting the training loss of instance  $i$  by a small amount  $\epsilon$ , i.e., of changing the empirical risk from the full-dataset risk  $R(\mathcal{D}; \boldsymbol{\theta})$  to  $R(\mathcal{D}; \boldsymbol{\theta}) - \epsilon L(\mathbf{z}_i; \boldsymbol{\theta})$ . We use  $\mathcal{D}_{-i,\epsilon}$  to denote this down-weighted dataset. We apply the implicit function theorem to the stationary point condition for (4) to derive the following (proof in Appendix B.2).

**Proposition 1.** *Given Assumption 1, the parameter change due to down-weighting training instance  $\mathbf{z}_i$  by an amount  $\epsilon$  is approximated by influence functions as*

$$\widehat{\Delta\boldsymbol{\theta}}(\mathcal{D}_{-i,\epsilon}) - \widehat{\Delta\boldsymbol{\theta}}(\mathcal{D}) \approx \epsilon \left( \mathbf{H}(\boldsymbol{\theta}^f) + \lambda \mathbf{I} \right)^{-1} \left( \nabla_{\boldsymbol{\theta}} L(\mathbf{z}_i; \boldsymbol{\theta}^f) + \nabla_{\boldsymbol{\theta}}^2 L(\mathbf{z}_i; \boldsymbol{\theta}^f) \widehat{\Delta\boldsymbol{\theta}}(\mathcal{D}) \right), \quad (7)$$

where  $\mathbf{H}(\boldsymbol{\theta}^f) = \nabla_{\boldsymbol{\theta}}^2 R(\mathcal{D}; \boldsymbol{\theta}^f)$  is the Hessian of the full-dataset empirical risk evaluated at  $\boldsymbol{\theta}^f$ .

If  $\boldsymbol{\theta}^f$  is a stationary point of the full-dataset risk  $R(\mathcal{D}; \boldsymbol{\theta})$ , then  $\Delta\boldsymbol{\theta}(\mathcal{D}) = \widehat{\Delta\boldsymbol{\theta}}(\mathcal{D}) = \mathbf{0}$  and (7) reduces to the familiar inverse Hessian-gradient product (with damping):

$$\widehat{\Delta\boldsymbol{\theta}}(\mathcal{D}_{-i,\epsilon}) \approx \epsilon \left( \mathbf{H}(\boldsymbol{\theta}^f) + \lambda \mathbf{I} \right)^{-1} \nabla_{\boldsymbol{\theta}} L(\mathbf{z}_i; \boldsymbol{\theta}^f). \quad (8)$$

If  $\boldsymbol{\theta}^f$  is not stationary however, then  $\widehat{\Delta\boldsymbol{\theta}}(\mathcal{D}) \neq \mathbf{0}$  as discussed in Section 3. Previous works like Koh and Liang (2017) still neglect the last  $\widehat{\Delta\boldsymbol{\theta}}(\mathcal{D})$  term in (7), arguing that if  $\boldsymbol{\theta}^f$  is near-stationary, then  $\widehat{\Delta\boldsymbol{\theta}}(\mathcal{D})$  is small and the product  $\epsilon \widehat{\Delta\boldsymbol{\theta}}(\mathcal{D})$  is second-order. It is also convenient to neglect this  $\widehat{\Delta\boldsymbol{\theta}}(\mathcal{D})$  term because one would otherwise have to compute  $\widehat{\Delta\boldsymbol{\theta}}(\mathcal{D})$ . We will neglect it as well in the present work to be consistent with previous TDA methods. In Appendices B.2 and B.3 however, we provide an expression for  $\widehat{\Delta\boldsymbol{\theta}}(\mathcal{D})$  and also show how to account for the  $\widehat{\Delta\boldsymbol{\theta}}(\mathcal{D})$  term in (7) without requiring the Hessian  $\nabla_{\boldsymbol{\theta}}^2 L(\mathbf{z}_i; \boldsymbol{\theta}^f)$ .

### 4.3.2 Gauss-Newton approximate Hessian

It is often the case that the loss function  $L(\mathbf{z}_i; \boldsymbol{\theta})$  is a composition  $\bar{\ell}(\bar{f}(\mathbf{z}_i; \boldsymbol{\theta}))$  of a *scalar-valued* model output function  $\bar{f}(\mathbf{z}_i; \boldsymbol{\theta})$  with a convex univariate loss function  $\bar{\ell}(\bar{f})$ . Here we allow  $\bar{f}(\mathbf{z}_i; \boldsymbol{\theta})$  to also depend on the target  $y_i$ . For example, if  $f(\mathbf{x}_i; \boldsymbol{\theta})$  is a regression model,  $\bar{f}(\mathbf{z}_i; \boldsymbol{\theta}) = f(\mathbf{x}_i; \boldsymbol{\theta}) - y_i$  can be the prediction error. For multi-class classification, Park et al. (2023) define  $\bar{f}(\mathbf{z}_i; \boldsymbol{\theta})$  to be the logit of the predicted probability of the target class  $y_i$ , which allows multi-class classification to be handled in the same way (see Section 3.3 of Park et al. (2023) for details).

Given the compositional form  $L(\mathbf{z}_i; \boldsymbol{\theta}) = \bar{\ell}(\bar{f}(\mathbf{z}_i; \boldsymbol{\theta}))$ , the gradient and Hessian of  $L(\mathbf{z}_i; \boldsymbol{\theta})$  are given by

$$\nabla_{\boldsymbol{\theta}} L(\mathbf{z}_i; \boldsymbol{\theta}) = \bar{\ell}'(\bar{f}(\mathbf{z}_i; \boldsymbol{\theta})) \nabla_{\boldsymbol{\theta}} \bar{f}(\mathbf{z}_i; \boldsymbol{\theta}), \quad (9)$$

$$\nabla_{\boldsymbol{\theta}}^2 L(\mathbf{z}_i; \boldsymbol{\theta}) = \bar{\ell}''(\bar{f}(\mathbf{z}_i; \boldsymbol{\theta})) \nabla_{\boldsymbol{\theta}} \bar{f}(\mathbf{z}_i; \boldsymbol{\theta}) \nabla_{\boldsymbol{\theta}} \bar{f}(\mathbf{z}_i; \boldsymbol{\theta})^T + \bar{\ell}'(\bar{f}(\mathbf{z}_i; \boldsymbol{\theta})) \nabla_{\boldsymbol{\theta}}^2 \bar{f}(\mathbf{z}_i; \boldsymbol{\theta}). \quad (10)$$

The Gauss-Newton approximation to the Hessian drops the second term in (10), which requires the Hessian  $\nabla_{\boldsymbol{\theta}}^2 \bar{f}(\mathbf{z}_i; \boldsymbol{\theta})$  that is more difficult to compute.

To obtain more compact expressions, let us define the gradient vectors  $\mathbf{g}_i = \nabla_{\boldsymbol{\theta}} \bar{f}(\mathbf{z}_i; \boldsymbol{\theta}^f)$ ,  $i = 1, \dots, n$  and matrix  $\mathbf{G} = [\mathbf{g}_1 \ \dots \ \mathbf{g}_n]^T$ , vector  $\mathbf{r} = -[\bar{\ell}'(\bar{f}(\mathbf{z}_1; \boldsymbol{\theta}^f)) \ \dots \ \bar{\ell}'(\bar{f}(\mathbf{z}_n; \boldsymbol{\theta}^f))]^T$ , and  $n \times n$  diagonal matrix  $\mathbf{V}$  with  $\bar{\ell}''(\bar{f}(\mathbf{z}_1; \boldsymbol{\theta}^f)), \dots, \bar{\ell}''(\bar{f}(\mathbf{z}_n; \boldsymbol{\theta}^f))$  as its diagonal entries. Using these definitions, (9), and the Gauss-Newton simplification of (10), the quadratic optimization in (4) can be rewritten for  $\mathcal{D}' = \mathcal{D}$  as

$$\min_{\Delta \boldsymbol{\theta}} -\mathbf{r}^T \mathbf{G} \Delta \boldsymbol{\theta} + \frac{1}{2} \Delta \boldsymbol{\theta}^T (\mathbf{G}^T \mathbf{V} \mathbf{G} + \lambda \mathbf{I}) \Delta \boldsymbol{\theta}. \quad (11)$$

where we have also disregarded the constant term.

The same derivation of influence functions in the proof of Proposition 1 applies to the Gauss-Newton approximation. Effectively, (9) and (10) (with the Gauss-Newton simplification) are used to substitute for the gradient and Hessian in (7).

**Corollary 1.** *Under the Gauss-Newton approximation, the influence function in Proposition 1 becomes*

$$\widehat{\Delta \boldsymbol{\theta}}(\mathcal{D}_{-i, \epsilon}) - \widehat{\Delta \boldsymbol{\theta}}(\mathcal{D}) \approx \epsilon \left( v_{ii} \mathbf{g}_i^T \widehat{\Delta \boldsymbol{\theta}}(\mathcal{D}) - r_i \right) (\mathbf{G}^T \mathbf{V} \mathbf{G} + \lambda \mathbf{I})^{-1} \mathbf{g}_i.$$

As with Proposition 1, this is a generalization of the standard influence function to non-stationary  $\boldsymbol{\theta}^f$  and non-zero  $\widehat{\Delta \boldsymbol{\theta}}(\mathcal{D})$ . It reduces to the standard form used in previous works when  $\widehat{\Delta \boldsymbol{\theta}}(\mathcal{D}) = \mathbf{0}$ :

$$\widehat{\Delta \boldsymbol{\theta}}(\mathcal{D}_{-i, \epsilon}) \approx -\epsilon r_i (\mathbf{G}^T \mathbf{V} \mathbf{G} + \lambda \mathbf{I})^{-1} \mathbf{g}_i. \quad (12)$$

### 4.3.3 Relationships with existing influence function methods

We now discuss how existing influence function methods correspond to the simplified versions (8) and (12) of Proposition 1 and Corollary 1. We refer to the cited works for more details on the methods.

**Conjugate gradient (CG) and LiSSA** Both (8) and (12) require computing an inverse Hessian-gradient product, with either the damped true Hessian  $\mathbf{H}(\boldsymbol{\theta}^f) + \lambda \mathbf{I}$  or the Gauss-Newton Hessian  $\mathbf{G}^T \mathbf{V} \mathbf{G} + \lambda \mathbf{I}$ . For models with a large number of parameters  $p$ , the  $O(p^3)$  computational cost of directly solving the system of equations is prohibitive. Koh and Liang (2017) proposed to apply CG (Martens, 2010) and LiSSA (Agarwal et al., 2017), two methods that approximate the solution iteratively. The former does so by applying the CG algorithm to an equivalent quadratic minimization problem, while the latter uses a truncated Neumann series. Both use repeated Hessian-vector products (HVPs) and can be applied to either (8) or (12).

**Arnoldi influence functions** Schioppa et al. (2022) propose to use Arnoldi iteration (a.k.a. Lanczos iteration for symmetric matrices) to approximately compute the largest-magnitude eigenvalues and corresponding eigenvectors of  $\mathbf{H}(\boldsymbol{\theta}^f)$ . The method then projects gradient vectors into the subspace of top eigenvectors of  $\mathbf{H}(\boldsymbol{\theta}^f)$ . By virtue of the orthonormal basis of eigenvectors for this subspace, the matrix inversion in (8) reduces to scalar division by eigenvalues.

The following methods are based on and therefore specific to the Gauss-Newton approximation.

**TRAK** TRAK (Park et al., 2023) can be seen as a hybrid TDA method that combines a gradient-based approximation with re-training (training an ensemble of models). Under the FiMO setting where re-training is not possible, we focus on the gradient-based part of TRAK by setting its parameter  $M$  (number of trained models) to 1. This variant, which we refer to as  $\text{TRAK}_{M=1}$ , falls under the Gauss-Newton framework of Section 4.3.2. First, TRAK applies a random projection matrix  $\mathbf{P} \sim \mathcal{N}(0, 1)^{p \times k}$  to reduce the dimensionality of the gradients:  $\boldsymbol{\phi}_i = \mathbf{P}^T \mathbf{g}_i$  and  $\boldsymbol{\Phi} = \mathbf{G}\mathbf{P}$ . With  $\boldsymbol{\phi}_i$  and  $\boldsymbol{\Phi}$  in place of  $\mathbf{g}_i$  and  $\mathbf{G}$ ,  $\text{TRAK}_{M=1}$  corresponds to a special case of (12) with  $\lambda = 0$  (no regularization) and  $\mathbf{V} = \mathbf{I}$  (non-identity  $\mathbf{V}$  found empirically to have little effect):<sup>3</sup>

$$\widehat{\Delta\boldsymbol{\theta}}_{\text{TRAK}}(\mathcal{D}_{-i}) = -r_i(\boldsymbol{\Phi}^T \boldsymbol{\Phi})^{-1} \boldsymbol{\phi}_i.$$

**EK-FAC** Grosse et al. (2023) start with the Gauss-Newton approximation in their work, corresponding to (12). Next, they adopt the K-FAC and EK-FAC approximations from Martens and Grosse (2015); George et al. (2018), which first approximate the Gauss-Newton Hessian as block-diagonal, where each block corresponds to a layer in a NN. This allows influence functions to be computed separately for each layer. Then for certain layers, an uncorrelatedness assumption is made that permits a Kronecker factorization of the corresponding block of the Hessian, making inversion much more efficient.

**DataInf** Kwon et al. (2024) start with a variant of the Gauss-Newton approximation in which  $\bar{\ell}(\bar{f}) = \bar{f}$  is the identity function and  $\mathbf{g}_i = \nabla_{\boldsymbol{\theta}} L(\mathbf{z}_i; \boldsymbol{\theta}^f)$  is a gradient of the loss. They then make the same block-diagonal/layer-wise approximation as Grosse et al. (2023). Setting this simplification aside, DataInf corresponds to (12) with  $r_i = -1$  (identity  $\bar{\ell}$ ) and  $\mathbf{V} = (1/n)\mathbf{I}$  (identity  $\bar{\ell}$ , average over  $\mathcal{D}$  instead of sum). The result is  $\widehat{\Delta\boldsymbol{\theta}}(\mathcal{D}_{-i}) = ((1/n)\mathbf{G}^T \mathbf{G} + \lambda \mathbf{I})^{-1} \mathbf{g}_i$ . The key idea of DataInf is to then interchange the order of averaging and matrix inversion, i.e.,

$$\left(\frac{1}{n}\mathbf{G}^T \mathbf{G} + \lambda \mathbf{I}\right)^{-1} = \left(\frac{1}{n}\sum_{i=1}^n \mathbf{g}_i \mathbf{g}_i^T + \lambda \mathbf{I}\right)^{-1} \approx \frac{1}{n}\sum_{i=1}^n (\mathbf{g}_i \mathbf{g}_i^T + \lambda \mathbf{I})^{-1}.$$

They then use the Sherman-Morrison formula to express  $(\mathbf{g}_i \mathbf{g}_i^T + \lambda \mathbf{I})^{-1}$  in closed form, resulting in an approximation to (5) that involves only gradient inner products.

## 5 Related Work

This work builds upon existing works that also take a retrospective look at TDA methods, and influence functions in particular (Basu et al., 2021; Zhang and Zhang, 2022; Bae et al., 2022; Schioppa

<sup>3</sup>Park et al. (2023) actually begin with an exact leave-one-out formula but find that the denominator also has little effect.



et al., 2023; Nguyen et al., 2023). We discuss individual papers more deeply in Appendix C. Here, we note the key differences between our work and these prior works:

1. **More gradient-based methods:** Our unified view (Section 4) and numerical comparisons (Section 6) encompass gradient-based methods beyond influence functions, including more recent methods such as TRAK and DataInf as well as first-order methods. We thereby obtain insights into similarities and differences among gradient-based methods, in addition to their performance on a task (approximation of further training in our case). In contrast, Basu et al. (2021); Zhang and Zhang (2022); Bae et al. (2022); Schioppa et al. (2023) mainly focus on influence functions, while Nguyen et al. (2023) evaluate fewer methods than we do.
2. **Further training:** The further training gold standard in Section 3 formalizes similar procedures used in previous works (in Appendix D.2 in Bae et al. (2022), in the experiment in Section 5.2 of Schioppa et al. (2023)). The proposal of averaging over realizations of stochastic further training appears to be new, and our results in Figure 3 show that it brings further training closer to what gradient-based methods estimate. Bae et al. (2022) propose an alternative gold standard called the proximal Bregman response function (PBRF). The PBRF however involves a non-standard Bregman distance objective, tailored specifically to be closer to influence functions, whereas our further training is more generic.
3. **FiMO setting:** We explicitly define the FiMO setting, which these previous works have not.

## 6 Numerical Comparison of Gradient-Based Methods to Further Training

In Section 4, we showed that many gradient-based TDA methods are approximations to further training in the FiMO setting. We now report on experiments that assess the quality of these approximations.

### 6.1 Experimental setup

We refer to Appendix D for more details on data, training, computation, the evaluation metric, etc.

**Datasets** Our experiments span the modalities of tabular, image, and text data. However, since we aimed to implement the further training gold standard described in Section 3, which is computationally expensive, our experiments are most comprehensive in the tabular case. We used four tabular datasets: two for regression, Concrete Strength and Energy Efficiency from the UCI repository (Kelly et al.) following Bae et al. (2022), and two larger ones for classification, FICO Challenge (FICO, 2018) and Folktables (Ding et al., 2021). For image data, we chose the CIFAR-10 image classification dataset (Krizhevsky, 2009), while for text, we used the SST-2 sentiment classification dataset (Socher et al., 2013), which is part of the GLUE benchmark (Wang et al., 2019).

**“Final” Models** For all tabular datasets, we used a 2-hidden-layer multi-layer perceptron (MLP) with 128 units in each hidden layer. The MLPs were trained using stochastic gradient descent (SGD) to yield the final model  $f(\mathbf{x}, \boldsymbol{\theta}^f)$ . For CIFAR-10, we used a ResNet-9 architecture (He et al., 2015) and trained it using SGD. For SST-2, we fine-tuned a pre-trained BERT model (Devlin et al., 2019) using AdamW (Loshchilov and Hutter, 2019).

**Selection of test and training instances** Our aim was to estimate influence scores of a subset  $\mathcal{L} \subset \mathcal{D}$  of training instances on the losses of a subset of  $m$  test instances. Thus, the evaluation function was the loss,  $g(\mathbf{z}, \boldsymbol{\theta}) = L(\mathbf{z}; \boldsymbol{\theta})$ . For the Concrete and Energy datasets, we considered all test instances, while for the other datasets, we selected  $m = 100$  test instances at random. The training subset  $\mathcal{L}$  was also selected randomly with  $l = |\mathcal{L}| = 100$  for the tabular datasets and  $l = 50$  for CIFAR-10 and SST-2.

**Implementation of further training** For the results in this section, the further training algorithm  $A'$  is the same as  $A$ , i.e., AdamW for BERT and SGD otherwise. Appendix E has results on the tabular datasets using Adam as  $A'$  instead. We evaluated the approximation quality of gradient-based methods as a function of the amount of further training (epochs or steps). To approximate the expectation over  $\xi$  in (3), we took averages over  $r = 100$  random seeds (denoted as realizations  $\xi^{(s)}$  in (13) below), which control the order of instances in each training epoch.

We considered two methods for adjusting for the effect of further training alone. The first is as specified in (2), (3), i.e., subtracting the output due to further training on the full dataset  $\mathcal{D}$ . We found however that for some datasets, this adjustment left a non-negligible bias that varies from epoch to epoch, resulting in noisy cosine similarities. Please see Appendices D.3 and E for further discussion of and results from this first method. The second method (used in this section) subtracts the mean of the effects due to each LOO dataset  $\mathcal{D}_{-i}$ . Incorporating also the averaging over random seeds, the “gold” attribution score from further training is thus

$$a_i = \frac{1}{r} \sum_{s=1}^r \left[ g(\mathbf{z}, \boldsymbol{\theta}^f + \Delta\boldsymbol{\theta}(\mathcal{D}_{-i}, \xi^{(s)})) - \frac{1}{l} \sum_{i' \in \mathcal{L}} g(\mathbf{z}, \boldsymbol{\theta}^f + \Delta\boldsymbol{\theta}(\mathcal{D}_{-i'}, \xi^{(s)})) \right]. \quad (13)$$

**Approximate TDA methods** We experimented with the first-order methods Grad-Dot (Charpiat et al., 2019) (final-checkpoint-only TracIn (Pruthi et al., 2020)) and Grad-Cos, and influence function methods CG and LiSSA (Agarwal et al., 2017; Koh and Liang, 2017), TRAK $_{M=1}$  (Park et al., 2023), EK-FAC (Grosse et al., 2023), and DataInf (Kwon et al., 2024). For LiSSA, we considered both the Gauss-Newton version ((12), referred to simply as “LiSSA”) as well as the true Hessian version ((8), LiSSA-H). For CG, only the Gauss-Newton version was used, while Gauss-Newton is the only choice for TRAK $_{M=1}$ , EK-FAC, and DataInf. CG could not be run on CIFAR-10 and SST-2 because it took too long, whereas LiSSA-H ran out of GPU memory on SST-2. We adapted TRAK for regression (see Appendix D.4).

**Evaluation metric** For each test instance evaluated, we have a vector  $\mathbf{a} \in \mathbb{R}^l$  of gold attribution scores from further training (13), and corresponding vectors  $\hat{\mathbf{a}}$  from gradient-based methods. We use the cosine similarity between  $\mathbf{a}$  and  $\hat{\mathbf{a}}$  as the evaluation metric.

## 6.2 Results

**Similarity vs. amount of further training** Figure 2 shows the cosine similarity between the attribution scores of gradient-based TDA methods and further training, as a function of the amount of further training. The curves represent the mean cosine similarity over the  $m$  test instances, while the shaded area corresponds to one standard error above and below.

We make the following observations:

- **First-order methods:** The two first-order methods, Grad-Dot and Grad-Cos, have cosine similarity curves that decay with the amount of further training. Grad-Dot is generally superior

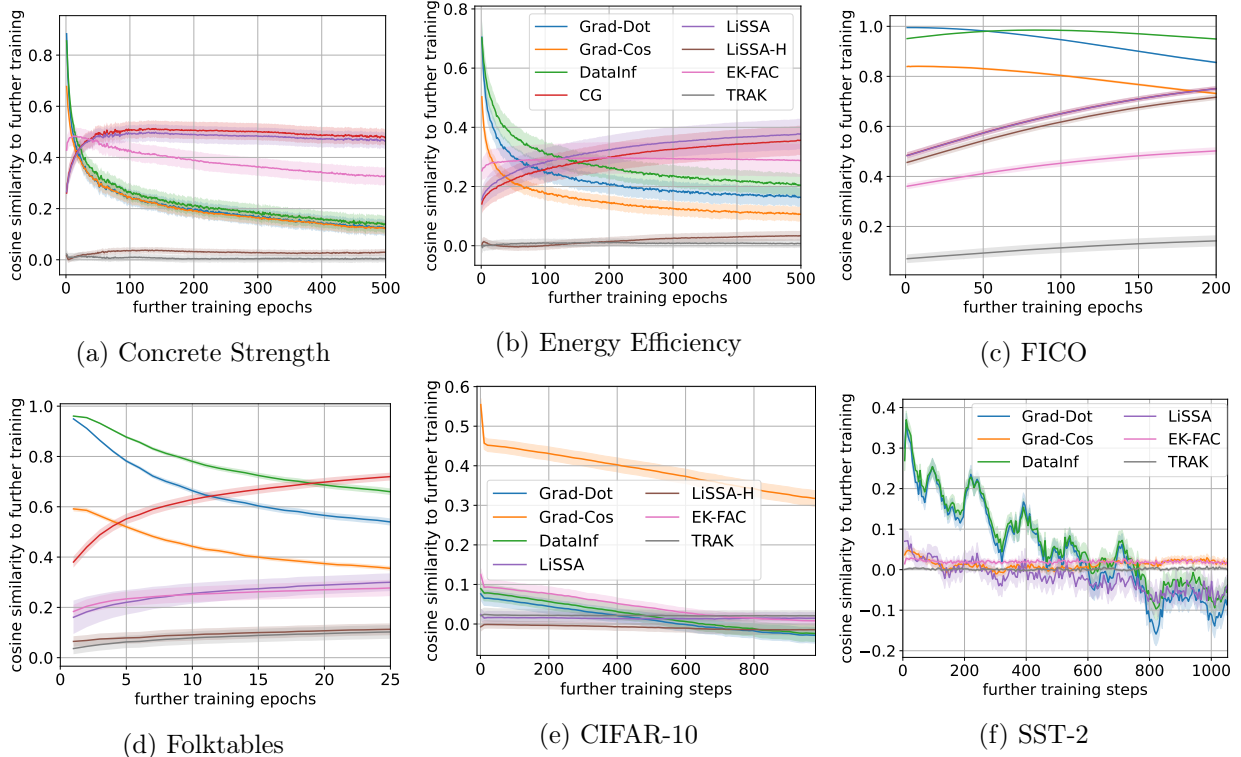


Figure 2: Cosine similarity between attribution scores of gradient-based TDA methods and further training, as a function of the number of epochs or steps of further training. The legend in panel (b) applies to (a)–(d). Note that in (c), CG overlaps almost perfectly with LiSSA.

to Grad-Cos, and the initial cosine similarity of the former is among the highest achieved by any approximate method. This aligns with Section 4.2 showing that Grad-Dot is the direct result of first-order approximation of further training, whereas the normalization of Grad-Cos is not supported by the theory. The notable exception is for CIFAR-10 (Figure 2e), which we comment on in Appendix E. The rate of decay after the initial peak varies with the dataset. One reason may be how far from stationary are the final model parameters  $\theta^f$ . If they are farther, then the parameter changes  $\Delta\theta(\mathcal{D})$  and  $\Delta\theta(\mathcal{D}_{-i})$  are larger, the first-order approximation is poorer, and the cosine similarity is thus lower.

- **DataInf:** We find it interesting that DataInf behaves like a first-order method, despite its attempt to incorporate second-order information. It is especially similar to Grad-Dot (cosine similarity between the two is typically above 0.95) and generally slightly higher in similarity to further training. We further interpret this similarity between DataInf and Grad-Dot in Appendix E.
- **CG, LiSSA, LiSSA-H:** Unlike the first-order methods, these influence function methods have cosine similarity curves that do not decay and may even increase with further training. However, they do not attain cosine similarities as high as the first-order methods (at least within the amount of further training that we conducted). A possible interpretation is that influence function methods provide better longer-range approximations to further training by using second-order information. However, the approximation may not be especially good at any point. Among the three methods, CG and LiSSA are similar to each other in the first

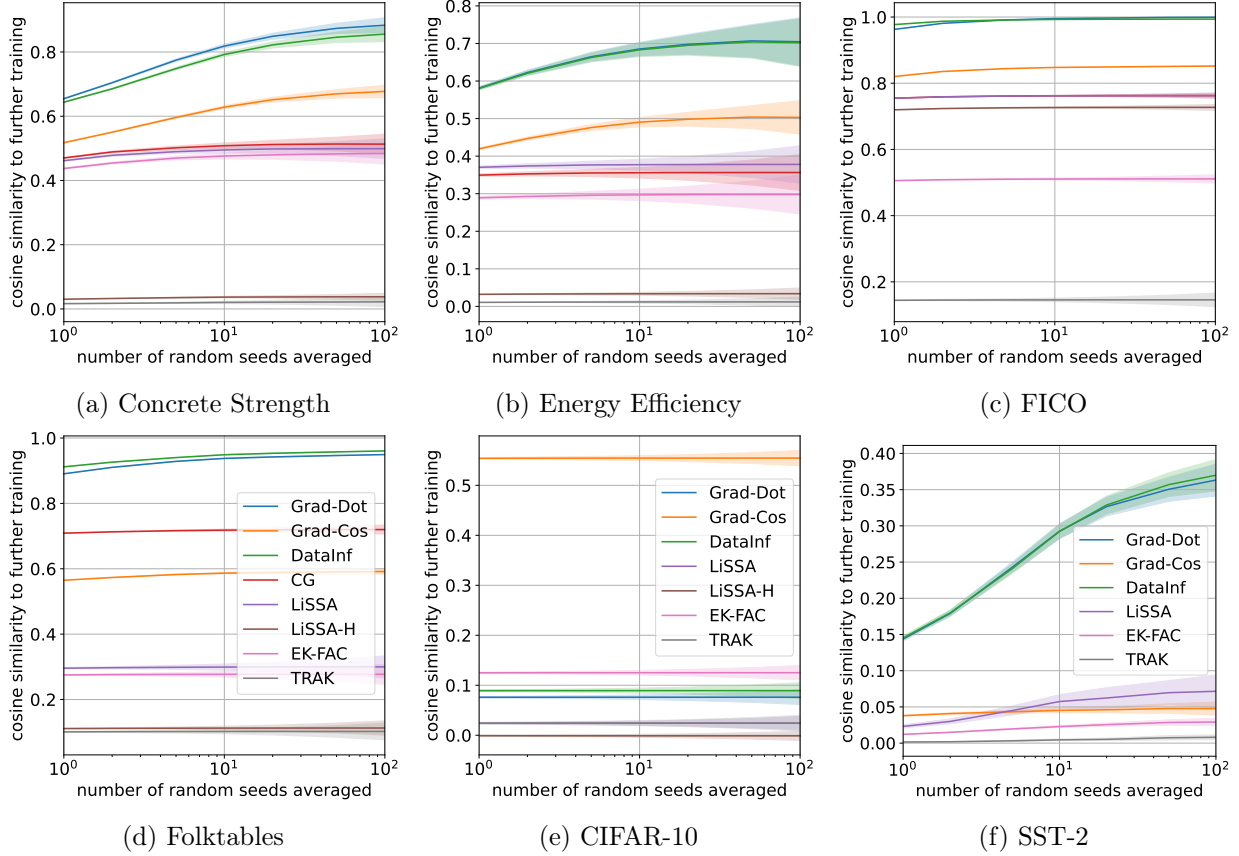


Figure 3: Maximum cosine similarity between attribution scores of gradient-based TDA methods and further training, as a function of the number of random seeds averaged.

row of Figure 2, but LiSSA seems to degrade in the second row as the model size increases. LiSSA-H on the other hand is consistently worse.

- **EK-FAC,  $\text{TRAK}_{M=1}$** : These are influence function methods that make additional approximations. Compared to LiSSA, EK-FAC has similar or higher cosine similarity in the second row of Figure 2, but is mostly worse in the first row.  $\text{TRAK}_{M=1}$  did not give good approximations to further training in any of our experiments.
- **CIFAR-10, SST-2**: The cosine similarities are significantly lower for these non-tabular datasets and models. The immediate reason for this is that the gold attribution vectors  $\mathbf{a}$  behave differently than they do for tabular data, as discussed in Appendix E.

**Similarity vs. amount of averaging** In Figure 3, we plot the maximum cosine similarity over epochs/steps (i.e., the maximum of each curve in Figure 2) as a function of the number  $r$  of random seeds averaged. The procedure is as follows. Given a number  $r$  of seeds to be averaged, we divide the 100 seeds that we have in total into  $100/r$  groups of  $r$  seeds. For each group of  $r$  seeds, we obtain a gold attribution vector  $\mathbf{a}$  using (13) and compute its cosine similarity with a gradient-based attribution vector  $\hat{\mathbf{a}}$ . We then compute means and standard errors of the cosine similarities over the  $m$  test instances as well as the  $100/r$  groups. This yields mean cosine similarities as a function of further training epochs or steps, like in Figure 2. Finally, we take the maximum over epochs or steps

to give us the  $y$ -axis value in Figure 3 corresponding to the number of seeds  $r$  on the  $x$ -axis. This procedure is repeated for different values of  $r$ .

In all cases in Figure 3, the cosine similarity increases with the number of seeds, implying that the averaging of further training runs brings it closer to what gradient-based methods estimate. This supports our proposal of averaging and its theoretical counterpart, the expectation in (3). While in some cases the increases are not visible in the plots, they are more notable for the first-order methods and DataInf, and for certain datasets like SST-2.

## 7 Conclusion

We have highlighted the final-model-only setting for TDA and proposed a further training gold standard for this setting. We then showed how several gradient-based TDA methods approximate further training in different ways, theoretically and numerically.

We note the following possibilities for future work:

- 1) Given the cosine similarity results in Figure 2, it is natural to hope for higher-quality approximate TDA methods, especially for non-tabular models. One possible starting point is the generalized influence function expressions in Proposition 1 and Corollary 1, which suggest a potential role for the parameter change  $\widehat{\Delta\theta}(\mathcal{D})$  from further training on the full dataset.
- 2) Figure 2 also suggests the question of whether the strengths of first- and second-order methods could be combined, i.e., higher initial similarity with less decay. We note that the damping parameter  $\lambda$  could be used to interpolate between first- and second-order methods.
- 3) Another open question is how much further training is the right amount to determine the final model’s sensitivity to training instances. If too little, the sensitivity may not be measurable, whereas if too much, then the measurement may no longer be local, i.e., specific to the given model  $f(\mathbf{x}; \theta^f)$ . The extent to which further training is well-approximated by Taylor expansions (as evaluated for example in Figure 2) may provide a partial answer.
- 4) We restricted attention in this work to LOO further training, as mentioned in Section 3. Future research on TDA in general could focus more on units larger than a single instance (referred to as “group influence” (Koh et al., 2019; Basu et al., 2020)), beyond making the additivity assumption that the attribution score for a group is the sum of LOO attribution scores.
- 5) While we have presented further training as applied to the original training set  $\mathcal{D}$  and assumed that  $\mathcal{D}$  is available, there is no obstacle to considering further training on new, unseen instances. This would change the problem from TDA to predicting the effect of further training on new data.

## Acknowledgements

We thank Swagatam Halder for early discussions on the TDA literature.

## References

- N. Agarwal, B. Bullins, and E. Hazan. Second-order stochastic optimization for machine learning in linear time. *Journal of Machine Learning Research*, 18(116):1–40, 2017. URL <http://jmlr.org/papers/v18/16-491.html>.

- J. Bae, N. Ng, A. Lo, M. Ghassemi, and R. B. Grosse. If influence functions are the answer, then what is the question? *Advances in Neural Information Processing Systems*, 35:17953–17967, 2022.
- J. Bae, W. Lin, J. Lorraine, and R. Grosse. Training data attribution via approximate unrolled differentiation, 2024. URL <https://arxiv.org/abs/2405.12186>. arXiv preprint arXiv:2405.12186.
- E. Barshan, M.-E. Brunet, and G. K. Dziugaite. RelatIF: Identifying explanatory training samples via relative influence. In *Proceedings of the Twenty Third International Conference on Artificial Intelligence and Statistics*, volume 108 of *Proceedings of Machine Learning Research*, pages 1899–1909. PMLR, 26–28 Aug 2020. URL <https://proceedings.mlr.press/v108/barshan20a.html>.
- S. Basu, X. You, and S. Feizi. On second-order group influence functions for black-box predictions. In *Proceedings of the 37th International Conference on Machine Learning*, volume 119 of *Proceedings of Machine Learning Research*, pages 715–724. PMLR, 13–18 Jul 2020. URL <https://proceedings.mlr.press/v119/basu20b.html>.
- S. Basu, P. Pope, and S. Feizi. Influence functions in deep learning are fragile. In *International Conference on Learning Representations (ICLR)*, 2021.
- G. Charpiat, N. Girard, L. Felardos, and Y. Tarabalka. Input similarity from the neural network perspective. In *Advances in Neural Information Processing Systems*, volume 32. Curran Associates, Inc., 2019. URL [https://proceedings.neurips.cc/paper\\_files/paper/2019/file/c61f571dbd2fb949d3fe5ae1608dd48b-Paper.pdf](https://proceedings.neurips.cc/paper_files/paper/2019/file/c61f571dbd2fb949d3fe5ae1608dd48b-Paper.pdf).
- Y. Chen, B. Li, H. Yu, P. Wu, and C. Miao. HyDRA: Hypergradient data relevance analysis for interpreting deep neural networks. *Proceedings of the AAAI Conference on Artificial Intelligence*, 35(8):7081–7089, May 2021. doi: 10.1609/aaai.v35i8.16871. URL <https://ojs.aaai.org/index.php/AAAI/article/view/16871>.
- A. R. Conn, N. I. M. Gould, and P. L. Toint. *Trust-region methods*. Society for Industrial and Applied Mathematics, USA, 2000. ISBN 0898714605.
- J. Devlin, M.-W. Chang, K. Lee, and K. Toutanova. BERT: Pre-training of deep bidirectional transformers for language understanding. In J. Burstein, C. Doran, and T. Solorio, editors, *Proceedings of the 2019 Conference of the North American Chapter of the Association for Computational Linguistics: Human Language Technologies, Volume 1 (Long and Short Papers)*, pages 4171–4186, Minneapolis, Minnesota, June 2019. Association for Computational Linguistics. doi: 10.18653/v1/N19-1423. URL <https://aclanthology.org/N19-1423>.
- F. Ding, M. Hardt, J. Miller, and L. Schmidt. Retiring adult: New datasets for fair machine learning. *Advances in Neural Information Processing Systems*, 34, 2021.
- V. Feldman and C. Zhang. What neural networks memorize and why: Discovering the long tail via influence estimation. In *Advances in Neural Information Processing Systems*, volume 33, pages 2881–2891. Curran Associates, Inc., 2020. URL [https://proceedings.neurips.cc/paper\\_files/paper/2020/file/1e14bfe2714193e7af5abc64ecbd6b46-Paper.pdf](https://proceedings.neurips.cc/paper_files/paper/2020/file/1e14bfe2714193e7af5abc64ecbd6b46-Paper.pdf).
- FICO. Explainable machine learning challenge, 2018. URL <https://community.fico.com/s/explainable-machine-learning-challenge?tabset-3158a=2>. <https://community.fico.com/s/explainable-machine-learning-challenge?tabset-3158a=2>.

- T. George, C. Laurent, X. Bouthillier, N. Ballas, and P. Vincent. Fast approximate natural gradient descent in a Kronecker factored eigenbasis. In *Advances in Neural Information Processing Systems*, volume 31. Curran Associates, Inc., 2018. URL [https://proceedings.neurips.cc/paper\\_files/paper/2018/file/48000647b315f6f00f913caa757a70b3-Paper.pdf](https://proceedings.neurips.cc/paper_files/paper/2018/file/48000647b315f6f00f913caa757a70b3-Paper.pdf).
- A. Ghorbani and J. Zou. Data Shapley: Equitable valuation of data for machine learning. In *Proceedings of the 36th International Conference on Machine Learning*, volume 97 of *Proceedings of Machine Learning Research*, pages 2242–2251. PMLR, 09–15 Jun 2019. URL <https://proceedings.mlr.press/v97/ghorbani19c.html>.
- A. Ghorbani, M. Kim, and J. Zou. A distributional framework for data valuation. In *Proceedings of the 37th International Conference on Machine Learning*, volume 119 of *Proceedings of Machine Learning Research*, pages 3535–3544. PMLR, 13–18 Jul 2020. URL <https://proceedings.mlr.press/v119/ghorbani20a.html>.
- R. Grosse, J. Bae, C. Anil, N. Elhage, A. Tamkin, A. Tajdini, B. Steiner, D. Li, E. Durmus, E. Perez, et al. Studying large language model generalization with influence functions. *arXiv preprint arXiv:2308.03296*, 2023.
- H. Guo, N. Rajani, P. Hase, M. Bansal, and C. Xiong. FastIF: Scalable influence functions for efficient model interpretation and debugging. In *Proceedings of the 2021 Conference on Empirical Methods in Natural Language Processing*, pages 10333–10350, Online and Punta Cana, Dominican Republic, Nov. 2021. Association for Computational Linguistics. doi: 10.18653/v1/2021.emnlp-main.808. URL <https://aclanthology.org/2021.emnlp-main.808>.
- Z. Hammoudeh and D. Lowd. Training data influence analysis and estimation: A survey. *Machine Learning*, 113(5):2351–2403, May 2024. URL <https://doi.org/10.1007/s10994-023-06495-7>.
- S. Hara, A. Nitanda, and T. Maehara. Data cleansing for models trained with SGD. In *Advances in Neural Information Processing Systems*, volume 32. Curran Associates, Inc., 2019. URL [https://proceedings.neurips.cc/paper\\_files/paper/2019/file/5f14615696649541a025d3d0f8e0447f-Paper.pdf](https://proceedings.neurips.cc/paper_files/paper/2019/file/5f14615696649541a025d3d0f8e0447f-Paper.pdf).
- K. He, X. Zhang, S. Ren, and J. Sun. Deep residual learning for image recognition. In *Intl. Conference on Computer Vision and Pattern Recognition (CVPR)*, 2015.
- A. Ilyas, S. M. Park, L. Engstrom, G. Leclerc, and A. Madry. Datamodels: Understanding predictions with data and data with predictions. In *Proceedings of the 39th International Conference on Machine Learning*, volume 162 of *Proceedings of Machine Learning Research*, pages 9525–9587. PMLR, 17–23 Jul 2022. URL <https://proceedings.mlr.press/v162/ilyas22a.html>.
- M. Kelly, R. Longjohn, and K. Nottingham. The UCI machine learning repository. URL <https://archive.ics.uci.edu>. <https://archive.ics.uci.edu>.
- P. W. Koh and P. Liang. Understanding black-box predictions via influence functions. In *International Conference on Machine Learning*, pages 1885–1894. PMLR, 2017.
- P. W. W. Koh, K.-S. Ang, H. Teo, and P. S. Liang. On the accuracy of influence functions for measuring group effects. In *Advances in Neural Information Processing Systems*, volume 32. Curran Associates, Inc., 2019. URL [https://proceedings.neurips.cc/paper\\_files/paper/2019/file/a78482ce76496fcf49085f2190e675b4-Paper.pdf](https://proceedings.neurips.cc/paper_files/paper/2019/file/a78482ce76496fcf49085f2190e675b4-Paper.pdf).

- A. Krizhevsky. Learning multiple layers of features from tiny images, 2009.
- Y. Kwon and J. Zou. Beta Shapley: A unified and noise-reduced data valuation framework for machine learning. In *Proceedings of The 25th International Conference on Artificial Intelligence and Statistics*, volume 151 of *Proceedings of Machine Learning Research*, pages 8780–8802. PMLR, 28–30 Mar 2022. URL <https://proceedings.mlr.press/v151/kwon22a.html>.
- Y. Kwon, E. Wu, K. Wu, and J. Zou. DataInf: Efficiently estimating data influence in loRA-tuned LLMs and diffusion models. In *The Twelfth International Conference on Learning Representations*, 2024. URL <https://openreview.net/forum?id=9m02ib92Wz>.
- J. Lin, A. Zhang, M. Lécuyer, J. Li, A. Panda, and S. Sen. Measuring the effect of training data on deep learning predictions via randomized experiments. In *Proceedings of the 39th International Conference on Machine Learning*, volume 162 of *Proceedings of Machine Learning Research*, pages 13468–13504. PMLR, 17–23 Jul 2022. URL <https://proceedings.mlr.press/v162/lin22h.html>.
- I. Loshchilov and F. Hutter. Decoupled weight decay regularization. In *International Conference on Learning Representations*, 2019. URL <https://openreview.net/forum?id=Bkg6RiCqY7>.
- J. Martens. Deep learning via Hessian-free optimization. In *Proceedings of the 27th International Conference on International Conference on Machine Learning*, ICML’10, page 735–742, Madison, WI, USA, 2010. Omnipress. ISBN 9781605589077.
- J. Martens and R. Grosse. Optimizing neural networks with Kronecker-factored approximate curvature. In *Proceedings of the 32nd International Conference on Machine Learning*, volume 37 of *Proceedings of Machine Learning Research*, pages 2408–2417, Lille, France, 07–09 Jul 2015. PMLR. URL <https://proceedings.mlr.press/v37/martens15.html>.
- E. Nguyen, M. Seo, and S. J. Oh. A Bayesian approach to analysing training data attribution in deep learning. *Advances in Neural Information Processing Systems*, 2023.
- S. M. Park, K. Georgiev, A. Ilyas, G. Leclerc, and A. Madry. TRAK: Attributing model behavior at scale. In *Proceedings of the 40th International Conference on Machine Learning*, volume 202 of *Proceedings of Machine Learning Research*, pages 27074–27113, 23–29 Jul 2023. URL <https://proceedings.mlr.press/v202/park23c.html>.
- A. Paszke, S. Gross, F. Massa, A. Lerer, J. Bradbury, G. Chanan, T. Killeen, Z. Lin, N. Gimelshein, L. Antiga, A. Desmaison, A. Köpf, E. Yang, Z. DeVito, M. Raison, A. Tejani, S. Chilamkurthy, B. Steiner, L. Fang, J. Bai, and S. Chintala. *PyTorch: an imperative style, high-performance deep learning library*. Curran Associates Inc., Red Hook, NY, USA, 2019.
- F. Pedregosa, G. Varoquaux, A. Gramfort, V. Michel, B. Thirion, O. Grisel, M. Blondel, P. Prettenhofer, R. Weiss, V. Dubourg, J. Vanderplas, A. Passos, D. Cournapeau, M. Brucher, M. Perrot, and E. Duchesnay. Scikit-learn: Machine learning in Python. *Journal of Machine Learning Research*, 12:2825–2830, 2011.
- G. Pruthi, F. Liu, S. Kale, and M. Sundararajan. Estimating training data influence by tracing gradient descent. *Advances in Neural Information Processing Systems*, 33:19920–19930, 2020.
- A. Schioppa, P. Zablotskaia, D. Vilar, and A. Sokolov. Scaling up influence functions. In *Proceedings of the AAAI Conference on Artificial Intelligence*, volume 36, pages 8179–8186, 2022.



- A. Schioppa, K. Filippova, I. Titov, and P. Zablotskaia. Theoretical and practical perspectives on what influence functions do. *Advances in Neural Information Processing Systems*, 36, 2023.
- O. Shamir and T. Zhang. Stochastic gradient descent for non-smooth optimization: Convergence results and optimal averaging schemes. In *Proceedings of the 30th International Conference on Machine Learning*, volume 28 of *Proceedings of Machine Learning Research*, pages 71–79, Atlanta, Georgia, USA, 17–19 Jun 2013. PMLR. URL <https://proceedings.mlr.press/v28/shamir13.html>.
- R. Socher, A. Perelygin, J. Wu, J. Chuang, C. D. Manning, A. Ng, and C. Potts. Recursive deep models for semantic compositionality over a sentiment treebank. In *Proceedings of the 2013 Conference on Empirical Methods in Natural Language Processing*, pages 1631–1642, Seattle, Washington, USA, Oct. 2013. Association for Computational Linguistics. URL <https://www.aclweb.org/anthology/D13-1170>.
- A. Wang, A. Singh, J. Michael, F. Hill, O. Levy, and S. R. Bowman. Glue: A multi-task benchmark and analysis platform for natural language understanding. In *Proceedings of the 24th International Conference on Learning Representations*, 2019.
- J. T. Wang and R. Jia. Data Banzhaf: A robust data valuation framework for machine learning. In *Proceedings of The 26th International Conference on Artificial Intelligence and Statistics*, volume 206 of *Proceedings of Machine Learning Research*, pages 6388–6421. PMLR, 25–27 Apr 2023. URL <https://proceedings.mlr.press/v206/wang23e.html>.
- D. Wei. Decision-making under selective labels: Optimal finite-domain policies and beyond. In *Proceedings of the 38th International Conference on Machine Learning*, volume 139 of *Proceedings of Machine Learning Research*, pages 11035–11046. PMLR, 18–24 Jul 2021. URL <https://proceedings.mlr.press/v139/wei21a.html>.
- C.-K. Yeh, J. Kim, I. E.-H. Yen, and P. K. Ravikumar. Representer point selection for explaining deep neural networks. In *Advances in Neural Information Processing Systems*, volume 31. Curran Associates, Inc., 2018. URL [https://proceedings.neurips.cc/paper\\_files/paper/2018/file/8a7129b8f3edd95b7d969dfc2c8e9d9d-Paper.pdf](https://proceedings.neurips.cc/paper_files/paper/2018/file/8a7129b8f3edd95b7d969dfc2c8e9d9d-Paper.pdf).
- R. Zhang and S. Zhang. Rethinking influence functions of neural networks in the over-parameterized regime. *Proceedings of the AAAI Conference on Artificial Intelligence*, 36(8):9082–9090, Jun. 2022. doi: 10.1609/aaai.v36i8.20893. URL <https://ojs.aaai.org/index.php/AAAI/article/view/20893>.

## A Further Training with Convex Objectives

For more classical models such as linear regression, logistic regression, and support vector machines, the empirical risk  $R(\mathcal{D}'; \theta)$  in the further training objective (1) is a convex function of the parameters  $\theta$ . If we further assume that  $R(\mathcal{D}'; \theta)$  is strictly convex in  $\theta$  (which is usually the case), then the exact minimizer is unique,

$$\theta^*(\mathcal{D}') = \arg \min_{\theta} R(\mathcal{D}'; \theta),$$

and barring numerical issues (for example with convex optimization solvers), we can tractably compute it. Moreover, it does not matter whether the optimization is initialized at initial parameter

values  $\boldsymbol{\theta}^{(0)}$  or trained parameters  $\boldsymbol{\theta}^f$ . Thus, further training and re-training become equivalent, provided that they are optimizing the same empirical risk.

Given the relative ease of obtaining the exact minimizer  $\boldsymbol{\theta}^*(\mathcal{D})$  on the full training set, it is reasonable to assume that any final, trained parameters have converged to it, i.e.,  $\boldsymbol{\theta}^f = \boldsymbol{\theta}^*(\mathcal{D})$ . In this case, there is no non-convergence problem as in Section 3, and further training would yield no change, i.e.,  $\Delta\boldsymbol{\theta}(\mathcal{D}) = \mathbf{0}$  in (1). As for stochastic training algorithms, they can of course also be applied to convex objectives, often with convergence guarantees (see e.g. Shamir and Zhang (2013) as one example among many). This greatly reduces the problem of stochasticity.

## B Approximate Further Training

### B.1 Regularization/damping term

The following reasons provide optimization-based justification for the  $\ell_2$  regularizer  $(\lambda/2)\|\Delta\boldsymbol{\theta}\|_2^2$  added in (4). This corresponds to the ‘‘damping’’ term  $\lambda\mathbf{I}$  added to the Hessian in estimating influence functions, where it is usually motivated simply as a means to ensure invertibility/positive definiteness.

1. **Enforce assumption/trust region:** Penalizing the  $\ell_2$  norm of  $\Delta\boldsymbol{\theta}$  enforces the assumption that  $\Delta\boldsymbol{\theta}$  is small. It can also be viewed as enforcing a *trust region* (Conn et al., 2000), a region around  $\boldsymbol{\theta}^f$  where the second-order expansion gives a better approximation.
2. **Ensure optimization is well-posed:** The loss function  $L(\mathbf{z}; \boldsymbol{\theta})$  for neural networks is typically non-convex, which implies that the empirical risk Hessian  $\nabla_{\boldsymbol{\theta}}^2 R(\mathcal{D}'; \boldsymbol{\theta}^f)$  may not be positive semidefinite. In the absence of the regularizer, if  $\nabla_{\boldsymbol{\theta}}^2 R(\mathcal{D}'; \boldsymbol{\theta}^f)$  has a negative eigenvalue, then the objective value in (4) would tend to  $-\infty$  in the direction of the corresponding eigenvector. If we add regularization with  $\lambda$  larger in magnitude than the most negative eigenvalue of  $\nabla_{\boldsymbol{\theta}}^2 R(\mathcal{D}'; \boldsymbol{\theta}^f)$ , then such divergence is prevented and an optimal solution to (4) exists. This consideration leads to Assumption 1.

### B.2 Proofs

*Proof of Proposition 1.* We substitute the down-weighted risk  $R(\mathcal{D}; \boldsymbol{\theta}) - \epsilon L(\mathbf{z}_i; \boldsymbol{\theta})$  for  $R(\mathcal{D}; \boldsymbol{\theta})$  everywhere in (4). Then the stationary point (i.e., zero-gradient) condition for (4) becomes

$$F(\epsilon, \Delta\boldsymbol{\theta}) \triangleq \nabla_{\boldsymbol{\theta}} R(\mathcal{D}; \boldsymbol{\theta}^f) - \epsilon \nabla_{\boldsymbol{\theta}} L(\mathbf{z}_i; \boldsymbol{\theta}^f) + \left( \mathbf{H}(\boldsymbol{\theta}^f) - \epsilon \nabla_{\boldsymbol{\theta}}^2 L(\mathbf{z}_i; \boldsymbol{\theta}^f) + \lambda \mathbf{I} \right) \Delta\boldsymbol{\theta} = \mathbf{0}. \quad (14)$$

For  $\epsilon = 0$ , i.e., no down-weighting, (14) is satisfied by the full-dataset parameter change

$$\widehat{\Delta\boldsymbol{\theta}}(\mathcal{D}) = - \left( \mathbf{H}(\boldsymbol{\theta}^f) + \lambda \mathbf{I} \right)^{-1} \nabla_{\boldsymbol{\theta}} R(\mathcal{D}; \boldsymbol{\theta}^f). \quad (15)$$

For small  $\epsilon$ , we apply the implicit function theorem to obtain an expression for  $\widehat{\Delta\boldsymbol{\theta}}(\mathcal{D}_{-i, \epsilon})$ . The relevant Jacobians of function  $F$  defined in (14) are

$$\begin{aligned} \mathbf{J}_{F, \Delta\boldsymbol{\theta}} &= \mathbf{H}(\boldsymbol{\theta}^f) - \epsilon \nabla_{\boldsymbol{\theta}}^2 L(\mathbf{z}_i; \boldsymbol{\theta}^f) + \lambda \mathbf{I}, \\ \mathbf{J}_{F, \epsilon} &= -\nabla_{\boldsymbol{\theta}} L(\mathbf{z}_i; \boldsymbol{\theta}^f) - \nabla_{\boldsymbol{\theta}}^2 L(\mathbf{z}_i; \boldsymbol{\theta}^f) \Delta\boldsymbol{\theta}, \end{aligned}$$

from which we obtain

$$\begin{aligned}\widehat{\Delta\theta}(\mathcal{D}_{-i,\epsilon}) - \widehat{\Delta\theta}(\mathcal{D}) &= -\epsilon \left( \mathbf{J}_{F,\Delta\theta} \Big|_{\epsilon=0, \Delta\theta=\widehat{\Delta\theta}(\mathcal{D})} \right)^{-1} \mathbf{J}_{F,\epsilon} \Big|_{\epsilon=0, \Delta\theta=\widehat{\Delta\theta}(\mathcal{D})} + O(\epsilon^2) \\ &\approx \epsilon \left( \mathbf{H}(\theta^f) + \lambda \mathbf{I} \right)^{-1} \left( \nabla_{\theta} L(\mathbf{z}_i; \theta^f) + \nabla_{\theta}^2 L(\mathbf{z}_i; \theta^f) \widehat{\Delta\theta}(\mathcal{D}) \right).\end{aligned}$$

□

*Proof of Corollary 1.* The result follows from (7) by substituting the Gauss-Newton Hessians  $\mathbf{H}(\theta^f) = \mathbf{G}^T \mathbf{V} \mathbf{G}$  and  $\nabla_{\theta}^2 L(\mathbf{z}_i; \theta^f) = v_{ii} \mathbf{g}_i \mathbf{g}_i^T$ ,  $\nabla_{\theta} L(\mathbf{z}_i; \theta^f) = -r_i \mathbf{g}_i$  from (9), and simplifying. □

### B.3 Simplification of Proposition 1 in the near-stationary case

If the final parameters  $\theta^f$  are near-stationary, then the parameter change  $\widehat{\Delta\theta}(\mathcal{D})$  in (7) is small. We may thus use a reverse Taylor expansion to approximate

$$\nabla_{\theta} L(\mathbf{z}_i; \theta^f) + \nabla_{\theta}^2 L(\mathbf{z}_i; \theta^f) \widehat{\Delta\theta}(\mathcal{D}) \approx \nabla_{\theta} L \left( \mathbf{z}_i; \theta^f + \widehat{\Delta\theta}(\mathcal{D}) \right),$$

which avoids computing the Hessian  $\nabla_{\theta}^2 L(\mathbf{z}_i; \theta^f)$ . Equation (7) becomes

$$\widehat{\Delta\theta}(\mathcal{D}_{-i,\epsilon}) - \widehat{\Delta\theta}(\mathcal{D}) \approx \epsilon \left( \mathbf{H}(\theta^f) + \lambda \mathbf{I} \right)^{-1} \nabla_{\theta} L \left( \mathbf{z}_i; \theta^f + \widehat{\Delta\theta}(\mathcal{D}) \right), \quad (16)$$

i.e., the gradient  $\nabla_{\theta} L(\mathbf{z}_i; \theta^f)$  in the standard influence function (8) is replaced with its counterpart after further training on  $\mathcal{D}$ . Moreover, (15) provides an expression for  $\widehat{\Delta\theta}(\mathcal{D})$  as a Newton step from  $\theta^f$ .

## C More on Related Work

In this appendix, we discuss some more closely related works individually.

Bae et al. (2022) examine the discrepancy between influence functions and leave-one-out re-training and decompose the discrepancy into five contributions. They show that influence functions are a much better approximation to a quantity they call the proximal Bregman response function (PBRF), which they propose as an alternative gold standard to LOO re-training. The key differences between our work and Bae et al. (2022) are as follows: 1) We propose further training based on standard training objectives (e.g., cross-entropy or mean squared error, no proximity regularization) as a different, more general gold standard. In contrast, the PBRF involves a non-standard Bregman distance objective, chosen specifically to be closer to influence functions. In their Appendix D.2, Bae et al. (2022) also discuss further training with and without leaving out one sample, which they refer to as “two-stage LOO re-training.” However, they do not consider taking an expectation over random trainings as we do. 2) Our unified view encompasses TDA methods beyond influence functions, including more recent methods such as TRAK (Park et al., 2023) and DataInf (Kwon et al., 2024) as well as first-order methods. We evaluate the extent to which all these methods approximate further training.

Schioppa et al. (2023) discuss problematic assumptions made by influence functions and TracIn (Pruthi et al., 2020) and how these can be addressed. They then show that the predictive power of influence functions and TracIn is fundamentally limited by divergence in parameters as (further) training proceeds. The latter contribution is the main point of connection with our work, where we also observe the fading of predictive power over training time, especially for first-order methods. The

differences in our work are: 1) We make explicit the further training gold standard that they compare to in their experiment (Schioppa et al., 2023, Sec. 5.2) and we further propose its expected version with respect to stochasticity in the training algorithm. 2) We conduct a larger-scale experiment than theirs in certain dimensions, notably the TDA methods evaluated, as well as averaging over the aforementioned stochasticity and using more test points and left-out training points.

Basu et al. (2021) show that influence functions become worse approximators of a training example’s importance on a test prediction with increasing model depth, width and if the models are trained with no weight decay. All experiments in the paper are conducted with further training (from the already trained model, not from scratch) determining the ground truth influence. However, Basu et al. (2021) do not average over further training realizations as we do. Moreover, their study is focused on influence functions, whereas we consider other gradient-based methods as well.

Nguyen et al. (2023) argue that a Bayesian approach is the correct way of evaluating influences of training examples on test predictions as there is a lot of variance in most TDA estimates when we account for random initialization of the model as well as variation in batching when training. In such situations the recommendation is to consider the distribution of attribution values for a training example, or at least consider the distribution’s variance, rather than simply (individual run) point estimates. Different from our work, the experiments in the paper are conducted by re-training models from scratch, and only three gradient-based TDA methods are studied, namely influence functions (IF), Grad-Dot (GD) and Grad-Cos (GC).

The seminal paper (Koh and Liang, 2017) on influence functions in ML sketched a derivation similar to ours in Section 4 and Appendix B, but in less detail. In particular, our more careful derivation of the influence function in Proposition 1 keeps the  $\widehat{\Delta\theta}(\mathcal{D})$  term that Koh and Liang (2017) neglect. Appendix B.1 also discusses the damping term  $\lambda\mathbf{I}$  at greater length.

Zhang and Zhang (2022) analyze the effectiveness of influence functions, but only for a 2-layer ReLU network. Moreover, the theoretical analysis is done w.r.t. the neural tangent kernel (NTK) approximation of the ReLU network. They have three key findings: i) Influence functions perform better as the width of the network increases. ii) Influence functions perform poorly with weak regularization, where the regularization tries to keep the model weights as close as possible to the initial weights. Our cosine similarity results in Figure 2 and elsewhere may be a reflection of this. iii) Influence functions perform better for examples that lie in the high density region of the training distribution.

## D Experimental Setup Details

### D.1 Data

**Choice of tabular datasets** We followed Bae et al. (2022) in using two regression datasets from the UCI repository (Kelly et al.), Concrete Compressive Strength and Energy Efficiency. We then departed from Bae et al. (2022) in choosing two classification datasets, FICO Challenge (FICO, 2018) and Folktables (Ding et al., 2021), because they are at least one order of magnitude larger than the tabular datasets in Bae et al. (2022) in terms of the number of instances and/or features.

**Data pre-processing** For Concrete, Energy, and FICO, we split the dataset 90%-10% into training and test sets (using the scikit-learn (Pedregosa et al., 2011) package’s `train_test_split()` with `random_state=0`) and standardized the features to have zero mean and unit variance. Handling of special feature values in FICO was done as in Wei (2021). For Folktables, we used the person-level data from year 2018 for the US state of Massachusetts. The classification task was predicting whether a person’s income is above or below USD 50,000 (task `ACSIncome`). The dataset was split 75%-25%

into training and test (again using `train_test_split()` with `random_state=0`), categorical features were dummy-coded, and numerical features were standardized. For CIFAR-10, we used the given split into training and test sets. We employed common data augmentation techniques such as random cropping and horizontal flipping, followed by standardization using the empirical mean and standard deviation of the training set. We used a random subset of 1000 samples as validation set. For SST-2, we used the given split into training, validation, and test sets. We drew the  $m = 100$  “test” instances for evaluation from the validation set because the actual test set lacks labels for computing losses. Text was tokenized using the tokenizer of the BERT model (see next subsection) with a maximum sequence length of 128 (more than sufficient for all SST-2 examples).

## D.2 Training of Final Models

**Tabular datasets** For all tabular datasets, we used a 2-hidden-layer multi-layer perceptron (MLP) with 128 units in each hidden layer. For the regression problems, the MLP has one output and the loss function is mean squared error (MSE), while for (binary) classification, the MLP has two outputs (logits) and the loss function is cross-entropy. The MLPs were trained using SGD for  $T = 1000$  epochs and a batch size of 128 (following Bae et al. (2022)) to yield the final model  $f(\mathbf{x}, \boldsymbol{\theta}^f)$ , except for the larger Folktables dataset where  $T = 100$ . Learning rates were as follows: 0.3 for Concrete and Energy, 0.001 for FICO, and 0.01 for Folktables.

**CIFAR-10** We used a ResNet-9 architecture (He et al., 2015) and trained it using SGD to minimize cross-entropy loss on the CIFAR-10 training set for  $T = 50$  epochs. We trained with a batch size of 512, learning rate of 0.4, and weight decay of 0.001.

**SST-2** We used a pre-trained `bert-base-uncased` model<sup>4</sup> (Devlin et al., 2019) and attached a linear classification layer that maps the BERT model’s final representation of the CLS token to logits. We fine-tuned this model on the SST-2 training set using AdamW (Loshchilov and Hutter, 2019) to minimize cross-entropy loss, with a batch size of 64, learning rate of  $10^{-5}$ , zero weight decay, and gradient norm clipping at a threshold of 1. Accuracy on the SST-2 validation set was used to choose the number of epochs from a range of 1 to 30. This resulted in a final model with validation accuracy of 92.9% after epoch 19.

## D.3 Implementation of further training

**Optimizer and parameters** For the case in which the further training algorithm  $A'$  is the same as the initial training algorithm  $A$ , the learning rate for  $A'$  was chosen to be one order of magnitude smaller than that for  $A$ , i.e., 0.03 for Concrete and Energy,  $10^{-4}$  for FICO and Folktables, 0.04 for CIFAR-10,  $10^{-6}$  for SST-2. The reason is that the given parameters  $\boldsymbol{\theta}^f$  are closer to convergence than the initial parameters  $\boldsymbol{\theta}^{(0)}$ . The maximum number of epochs  $T'$  for  $A'$  was also chosen to be a fraction of  $T$ :  $T' = 500$  for Concrete and Energy following Bae et al. (2022),  $T' = 200$  for FICO,  $T' = 25$  for Folktables,  $T' = 10$  for CIFAR-10, and  $T' = 1$  for SST-2. Other parameters such as batch size were the same as for  $A$ . For the experiment on tabular data in which  $A'$  was Adam, smaller learning rates were used since Adam is a more powerful optimizer:  $10^{-4}$  for Concrete and Energy,  $10^{-6}$  for FICO and Folktables.

---

<sup>4</sup><https://huggingface.co/google-bert/bert-base-uncased>

**Random seeds** Regarding the random seeds (denoted as  $\xi^{(s)}$  in (13), (17)) that determine the order of instances in each epoch, this control was achieved in PyTorch (Paszke et al., 2019) as follows: First, the seed of a random number `Generator` object was set to a specified value (using `generator.manual_seed()`). Then, a `RandomSampler` object was instantiated with this `Generator` (`RandomSampler(generator=generator, ...)`), and a `DataLoader` was instantiated with the `RandomSampler` (`DataLoader(sampler=sampler, ...)`).

**Leaving out instances** To achieve the effect of leaving out one training instance  $\mathbf{z}_i$ , we followed Schioppa et al. (2023) in subtracting a second loss term  $L(\mathbf{z}_i; \boldsymbol{\theta})/n$  from the usual loss for *every* batch. The scaling by  $1/n$  (recall that  $n$  is the number of training instances) approximately cancels out the weight of instance  $\mathbf{z}_i$  in the usual loss. Denoting by  $B$  and  $n_B = \lceil n/B \rceil$  the batch size and number of batches per epoch, the weight of  $\mathbf{z}_i$  in the usual loss is  $1/B$  (one appearance per epoch), whereas the total weight from the subtracted loss term is  $n_B/n \approx 1/B$ .

**Adjustment for the effect of further training alone** As discussed in Section 6.1, we investigated two methods for adjusting for the effect of further training alone, where the results in Figure 2 use the mean subtraction adjustment in (13). For the other adjustment method in which the output due to full-dataset training is subtracted, the attribution score is given by

$$v_i = \frac{1}{r} \sum_{s=1}^r \left[ g(\mathbf{z}, \boldsymbol{\theta}^f + \Delta\boldsymbol{\theta}(\mathcal{D}_{-i}, \xi^{(s)})) - g(\mathbf{z}, \boldsymbol{\theta}^f + \Delta\boldsymbol{\theta}(\mathcal{D}, \xi^{(s)})) \right]. \quad (17)$$

Results corresponding to (17) are shown in Figures 5 and 7.

## D.4 Approximate TDA methods

All methods take the final model  $f(\mathbf{x}; \boldsymbol{\theta}^f)$  as input, either by first computing its training loss gradients  $\nabla_{\boldsymbol{\theta}} L(\mathbf{z}_i; \boldsymbol{\theta}^f)$  and test loss gradients, or as a model object that is used to compute derivatives.

**Grad-Dot, Grad-Cos** Given the loss gradients, these are straightforward to implement as (normalized) inner products.

**CG, LiSSA, LiSSA-H** We used the implementations of these methods in the `torch-influence` repository<sup>5</sup> provided by Bae et al. (2022). For both CG and LiSSA, we used a damping value of  $\lambda = 0.01$ , which we found to yield higher cosine similarity values than the other  $\lambda = 0.001$  value used by Bae et al. (2022). We observed that cosine similarities increase as  $\lambda$  increases, so it is possible that further tuning of  $\lambda$  may yield better results. For LiSSA’s additional parameters, we set the `depth` (number of iterations) to 5000, the number of repeats (`repeat`) to 1, and the `scale` parameter to the smallest value in  $\{10, 20, 50, 100, 200, 500\}$  for which LiSSA did not diverge.

**DataInf** For the tabular datasets, we used the repository<sup>6</sup> provided by Kwon et al. (2024) with default parameter values, specifically `lambda_const_param=10` which determines the damping value. However for CIFAR-10 and SST-2, the authors’ code was not computationally efficient enough. Instead, we implemented DataInf’s key equation (Kwon et al., 2024, eq. (5)) ourselves. In doing so, we approximated the average over all training instances  $i = 1, \dots, n$  with an average over a random

<sup>5</sup><https://github.com/alstonlo/torch-influence>

<sup>6</sup><https://github.com/ykwon0407/DataInf>

subsample of size 1000. We also first computed the gradient inner products  $L_{l,i}$ ,  $L_{l,ik}$ ,  $L_{l,k}$  in their eq. (5) before computing eq. (5) itself.

**EK-FAC** We used the repository<sup>7</sup> corresponding to Grosse et al. (2023) with default parameter settings.

**TRAK** We used the repository<sup>8</sup> provided by Park et al. (2023) with default parameter settings. For the regression datasets Concrete and Energy, since the TRAK repository does not provide an implementation for regression, we tried to create one ourselves following their documentation.<sup>9</sup> For their “model output function,” we use the model’s prediction,  $f(\mathbf{x}; \boldsymbol{\theta})$  in our notation. The squared error loss is  $L(\mathbf{z}; \boldsymbol{\theta}) = \frac{1}{2}(f(\mathbf{x}; \boldsymbol{\theta}) - y)^2$ , so the output-to-loss gradient that TRAK also requires is

$$\frac{\partial L(\mathbf{z}; \boldsymbol{\theta})}{\partial f} = f(\mathbf{x}; \boldsymbol{\theta}) - y.$$

## D.5 Evaluation metric

The vectors  $\mathbf{a}$  of gold attribution scores and  $\hat{\mathbf{a}}$  of approximate attribution scores may have different scales. In this work, we do not concern ourselves with the differing scales, so we take both to be normalized to unit  $\ell_2$  norm. In this case, the squared Euclidean distance  $\|\hat{\mathbf{v}} - \mathbf{v}\|^2$  and cosine similarity  $\hat{\mathbf{v}}^T \mathbf{v}$  are equivalent up to an affine transformation, and we use the latter as the evaluation metric. Note that cosine similarity is a more demanding measure than Pearson correlation (used for example in Schioppa et al. (2023); Bae et al. (2022)), since the latter corresponds to approximating each gold score  $a_i$  by  $\alpha \hat{a}_i + \beta$  where  $\beta$  is a non-zero bias, whereas the former constrains  $\beta$  to be zero.

## D.6 Computing infrastructure

Experiments were run on an internal computing cluster providing nodes with 32 GB of CPU memory, V100 GPUs with 32 GB of GPU memory, and occasionally A100 GPUs with 40 or 80 GB of GPU memory. One CPU and one GPU were used at a time.

## E Additional Experimental Results and Discussion

**Similarity between Grad-Dot and DataInf** We reproduce DataInf’s key equation (Kwon et al., 2024, eq. (5)) below (with a sign change to be consistent with Section 4):

$$\hat{a}_k^{\text{DataInf}} = \sum_{l=1}^L \frac{1}{\lambda_l} \left( L_{l,k} - \frac{1}{n} \sum_{i=1}^n \frac{L_{l,i}}{\lambda_l + L_{l,ii}} L_{l,ik} \right), \quad (18)$$

where  $k$  indexes the training instance being attributed to,  $l$  the layers of the NN, and  $i$  all training instances.  $L_{l,i}$  and  $L_{l,ik}$  are inner products between layer-specific loss gradients, as defined in Kwon et al. (2024). The first term in (18) is like Grad-Dot (6) but with a layer-dependent weighting  $1/\lambda_l$ . The remaining average over  $i$  can be seen as a correction term. Our results in Figures 2–5 suggest that this correction term is small.

<sup>7</sup><https://github.com/pomonam/kronfluence>

<sup>8</sup><https://github.com/MadryLab/trak>

<sup>9</sup><https://trak.readthedocs.io/en/latest/modeloutput.html>

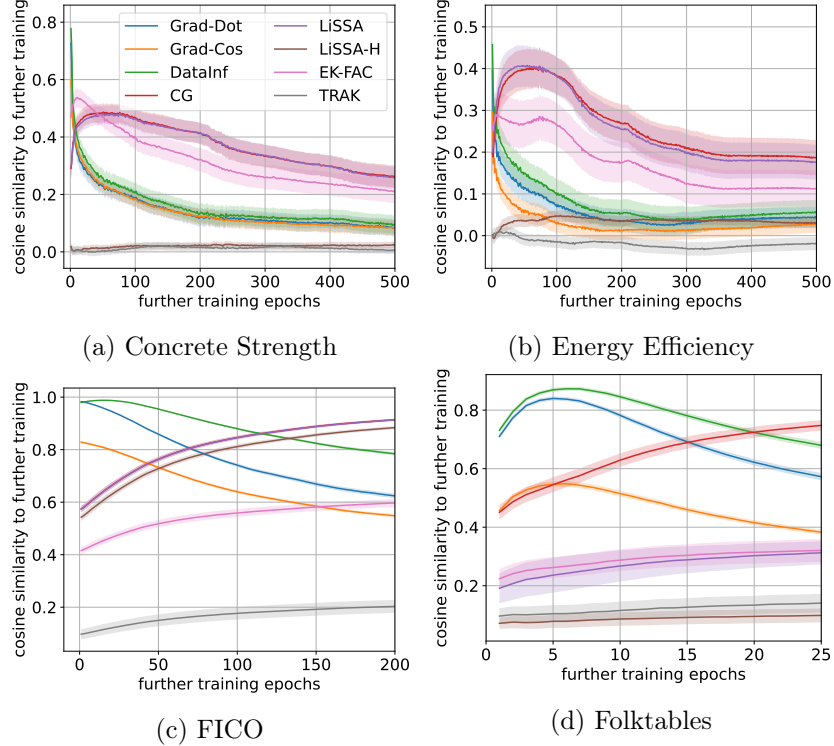


Figure 4: Cosine similarity between attribution scores of gradient-based TDA methods and further training as a function of the amount of further training, using a different further training algorithm (Adam) than the initial training algorithm (SGD).

**Different further training algorithm** Figure 4 shows the cosine similarity between attribution scores of gradient-based methods and further training for the tabular datasets, using Adam as the further training algorithm  $A'$  instead of SGD as in Figure 2. The patterns are broadly similar to those in Figure 2. However, for Folktables in Figure 4d, the curves for the first-order methods and DataInf do not peak at the beginning but rather after a few epochs. In Figures 4a and 4b, the curves for the influence function methods CG and LiSSA are also seen to peak and then decay.

**Different adjustment for the effect of further training alone** In Figure 5, the further training optimizer is the same as in Figure 2 ( $A' = A$ ), but the adjustment for the effect of further training alone is done using (17), i.e., by subtracting the output from full-dataset training. The plots for Concrete, Energy, FICO, and CIFAR-10 are similar to their counterparts in Figure 2. However for Folktables and SST-2 in Figure 5d, 5f, the curves are very noisy. The reason is that the adjustment in (17) still leaves a non-negligible constant bias, i.e., the attribution scores  $a_i$  are shifted up or down by a constant that varies from epoch to epoch. This varying bias is reflected in the cosine similarities shown in Figure 5d, 5f.



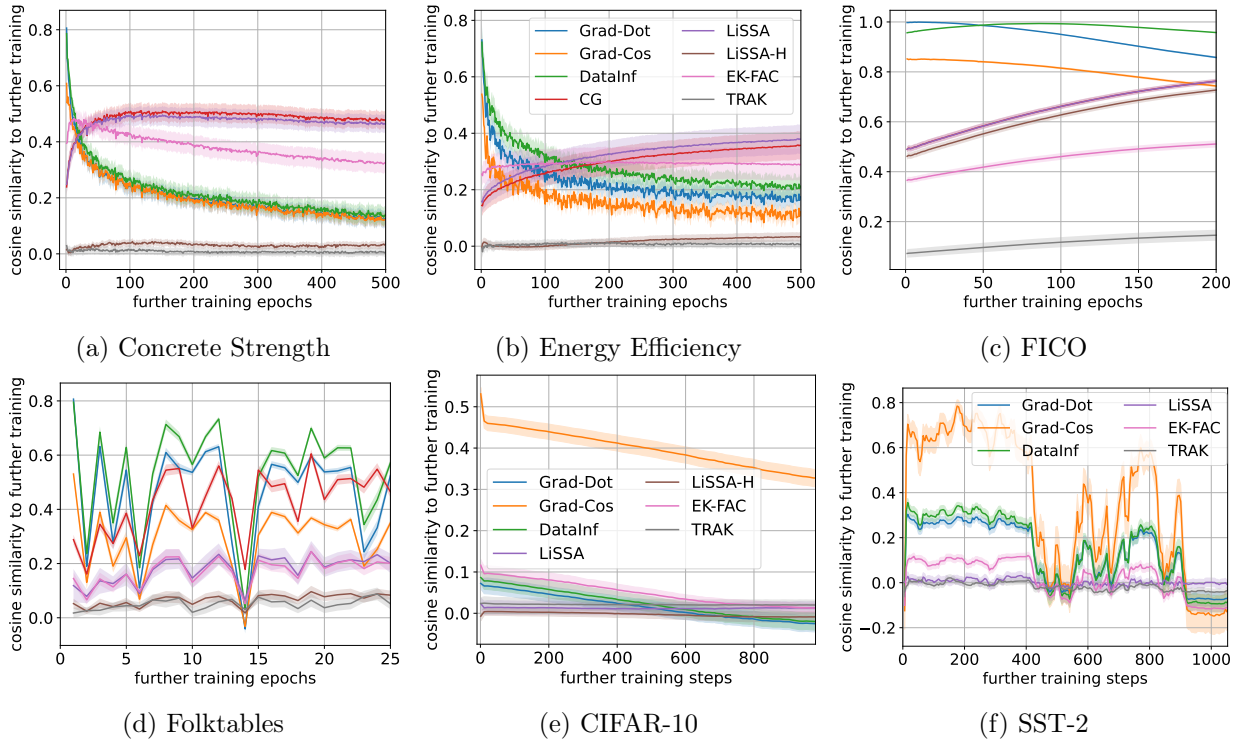


Figure 5: Cosine similarity between attribution scores of gradient-based TDA methods and further training using the same further training algorithms as in Figure 2, but with adjustment done according to (17).

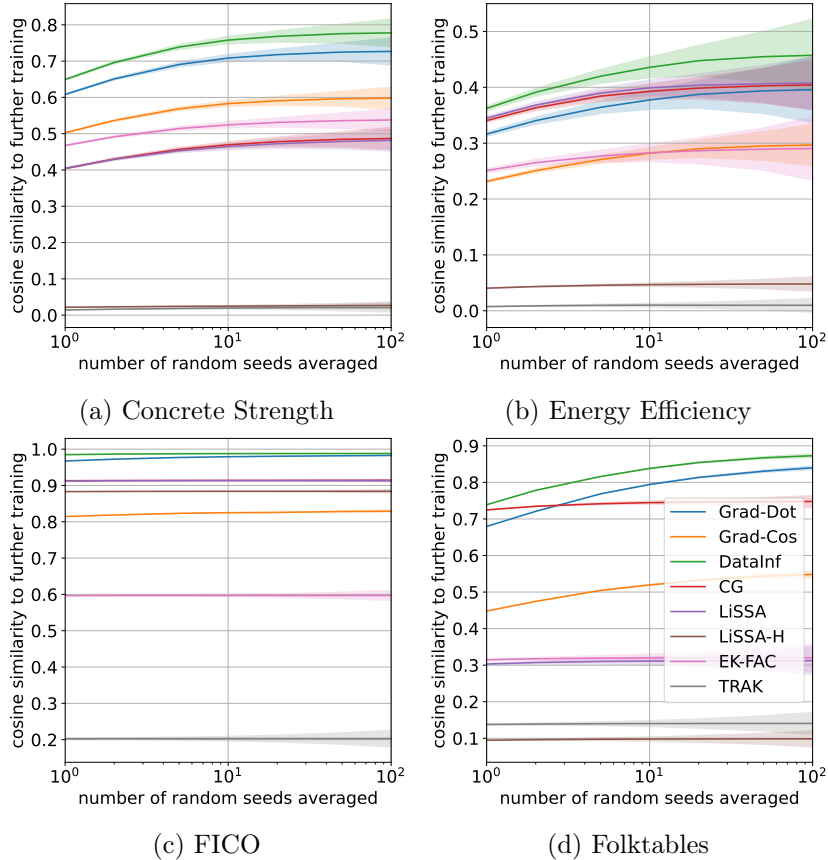


Figure 6: Maximum cosine similarity between attribution scores of gradient-based TDA methods and further training, as a function of the number of random seeds averaged. Here the further training algorithm (Adam) is different from the initial training algorithm (SGD).

**Different numbers of random seeds averaged** In Figures 6 and 7, we show the counterparts to Figure 3 when further training is done with Adam and when adjustment is done using (17), respectively. As in Figure 3, the cosine similarity increases in all cases with the number of seeds, implying that the averaging of further training brings it closer to what gradient-based methods estimate. The increases are especially notable in Figure 7 when adjustment is done using full-dataset further training (17). As seen in Figure 5, this adjustment method is noisier and appears to benefit more from averaging.

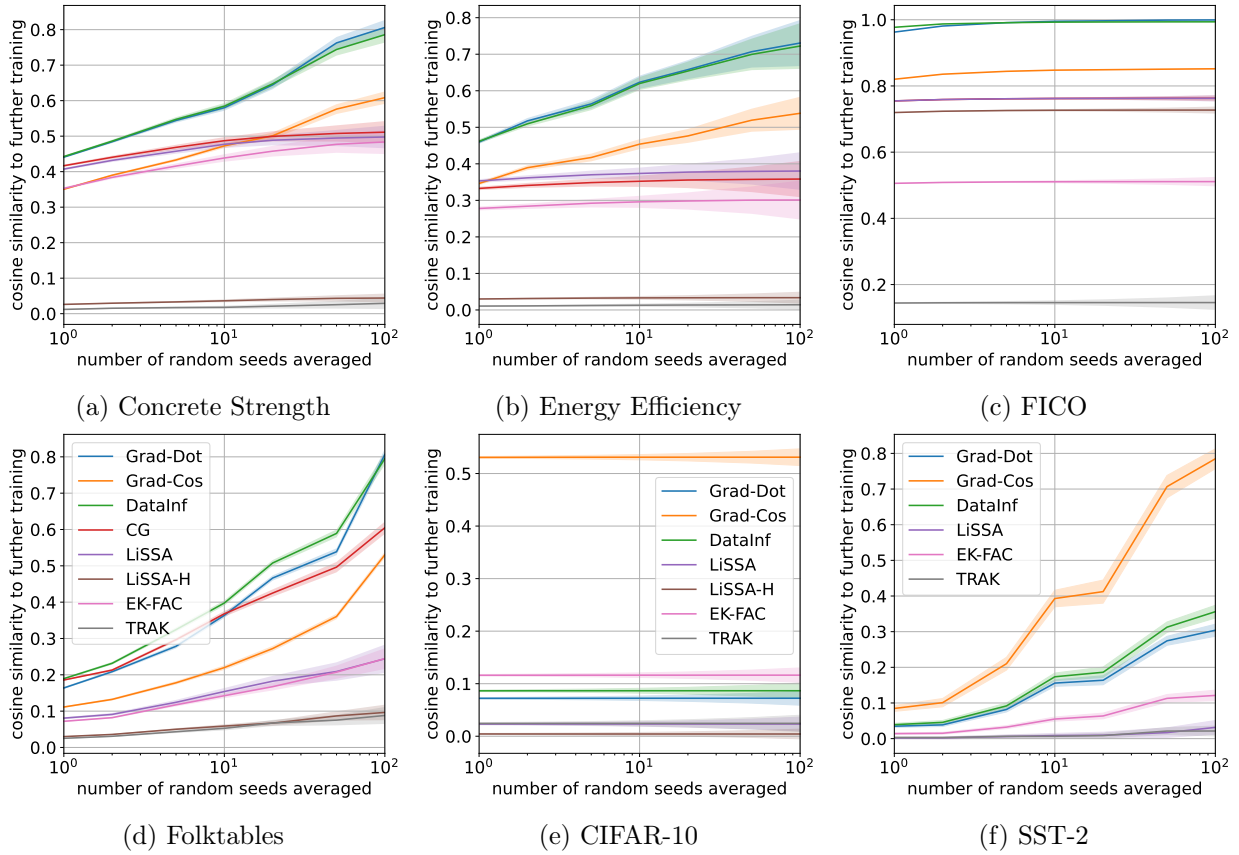


Figure 7: Maximum cosine similarity between attribution scores of gradient-based TDA methods and further training using full-dataset adjustment (17), as a function of the number of random seeds averaged.

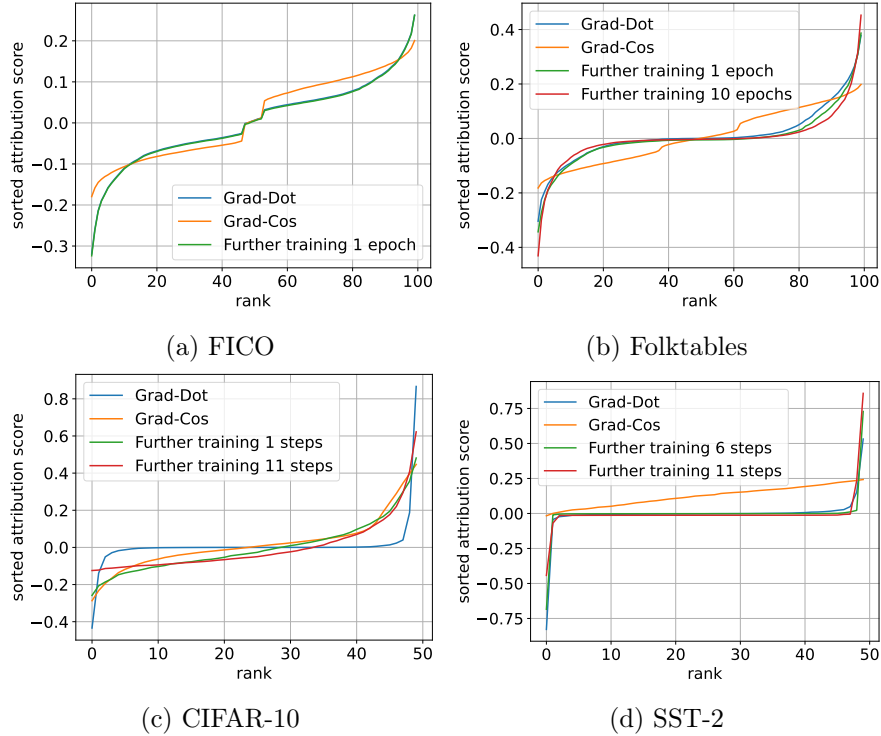


Figure 8: Attribution scores, sorted and averaged over test instances, from further training as well as Grad-Dot and Grad-Cos.

**CIFAR-10 and SST-2** The cosine similarities for CIFAR-10 and SST-2 in Figures 2e, 2f and elsewhere are significantly lower than those for the tabular datasets. As a first step to understanding why, we plot in Figure 8 the gold attribution scores from further training (13), where for each test instance, we have sorted the scores  $a_i$  in increasing order, and then averaged over the  $m$  test instances. We also sort and average the attribution scores from Grad-Dot and Grad-Cos in the same manner. For FICO and Folktables in Figures 8a, 8b, the further training attribution scores are more “typical” in that they are approximately symmetric (positive versus negative) and have tails of larger positive and negative values. For CIFAR-10 however (Figure 8c), the curves are more “hockey-stick”-shaped, with a heavier positive tail and not much of a negative tail; this pattern becomes more pronounced after 11 steps of further training than after 1 step. In this case, the Grad-Cos curve offers a better match than the Grad-Dot one. For SST-2, the gold attribution score curves are angular: almost all of the scores are close to zero, with only one or two significant non-zero values at either end. In both Figures 8c and 8d, Grad-Dot and Grad-Cos struggle more to approximate these less typical attribution score curves. Further investigation into the poorer approximation quality is ongoing.